General Disclaimer

One or more of the Following Statements may affect this Document

- This document has been reproduced from the best copy furnished by the organizational source. It is being released in the interest of making available as much information as possible.

- This document may contain data, which exceeds the sheet parameters. It was furnished in this condition by the organizational source and is the best copy available.

- This document may contain tone-on-tone or color graphs, charts and/or pictures, which have been reproduced in black and white.

- This document is paginated as submitted by the original source.

- Portions of this document are not fully legible due to the historical nature of some of the material. However, it is the best reproduction available from the original submission.

Report No. TE4073-146-68

Thermo Electron Corporation, 85 First Avenue, Waltham, Massachusetts 02154

FINAL REPORT

SIX-CONVERTER SOLAR THERMIONIC GENERATOR

T. Athanis

P. Shefsiek

L. Lazaridis

June 1968

Contract No. 951770

Prepared for

Jet Propulsion Laboratory
Pasadena, California

Report No. TE4073-146-68

Thermo Electron Corporation, 85 First Avenue, Waltham, Massachusetts 02154

FINAL REPORT

SIX-CONVERTER SOLAR THERMIONIC GENERATOR

T. Athanis

P. Shefsiek

L. Lazaridis

June 1968

Contract No. 951770

Prepared for

Jet Propulsion Laboratory
Pasadena, California

This work was performed for the Jet Propulsion Laboratory, California Institute of Technology, as sponsored by the National Aeronautics and Space Administration under Contract NAS7-100.

This report contains information prepared by Thermo Electron Corporation under JPL subcontract. Its content is not necessarily endorsed by the Jet Propulsion Laboratory, California Institute of Technology, or the National Aeronautics and Space Administration.

FOREWORD

This report was prepared by Thermo Electron Corporation, Waltham, Massachusetts, under JPL Contract No. 951770/NAS7-100. The report covers the work performed from January 10, 1967, through March 31, 1968.

The work was administered under the direction of Mr. Owen Merrill, California Institute of Technology, Jet Propulsion Laboratory, Pasadena, California.

The Thermo Electron Corporation personnel that contributed to this work includes: L. Lazaridis (Project Manager), Dr. P. Brosens, T. Athanis, P. Shefsiek, P. Pantazelos and W. Robinson. This report is designated by Thermo Electron as Report No. 4073-146-68.

Publication of this report does not necessarily constitute JPL approval of the report's findings or conclusions. It is published only for the exchange and stimulation of ideas.

ABSTRACT

This report covers the work accomplished during a 15-month period originated on January 10, 1967 under JPL Contract No. 951770/NAS7-100.

During the reporting period a six-converter solar thermionic generator (JG-4) was designed, fabricated and subjected to preliminary evaluation, including performance tests of each converter prior to its mounting on the generator. Six additional thermionic converters similar to those used in the generator were fabricated and individually tested. With the exception of one, each of the twelve converters tested produced more than 36 watts of output power at 0.7 volt output voltage, and at 2000°K emitter temperature. The average power output per converter was 37.5 watts.

All converters have identical overall configuration, employing planar electrode geometry with a rhenium emitter (of about 2 cm^2 area), and a molybdenum collector separated by about 0.005 cm (2 mils) during operation.

Critical parts of each converter and of the generator in general were subjected to detailed design analysis and performance evaluation. A thorough investigation was performed to determine the heat flux distribution and temperature profiles, the heat transfer mechanisms, and the heat dissipation requirements in the generator.

TABLE OF CONTENTS

LIST OF ILLUSTRATIONS

LIST OF ILLUSTRATIONS (continued)

LIST OF TABLES

CHAPTER 1

INTRODUCTION AND SUMMARY

This is the final report of the work performed under Contract No. 951770/NAS 7-100 during the period from January 10, 1967 through March 31, 1968. The work reported herein involves the design, fabrication and preliminary test of a six-converter solar thermionic generator designated as JG-4. The generator is to operate in a solar energy concentrating system consisting of a parabolic mirror of 57-inch rim radius and a 69-inch focal length. The mirror generates a solar image in the form of a circular ellipsoid which at the focal plane of the mirror has a cross sectional area of about 0.885 square inches and a maximum energy of about 5000 watts. The design of the six converters is similar to that of the Series VIII converters that have been used in previous solar generators, but has been modified to be compatible with a 6-converter system. The converters have planar electrodes with a Re emitter and Mo collector. The electrode area is 2 cm^2. The converters are to operate at an emitter temperature of 2000°K at an interelectrode spacing of 2 mils. There were several main tasks in this program and they are summarized below:

1. A detailed review and evaluation was made of the original JG-4 design (discussed in detail in TECO Report No. TE18-66). This was proposed because recent tests conducted at JPL showed that solid Re emitters and Re sleeves were more reliable for extended operation than the Ta substrate pressure-bonded Re emitters and Ta sleeves

proposed in the original design. However, incorporating solid Re emitters into the converters of the generator required redesign of the generator cavity because of the lower thermal conductivity of Re. The new design has the rear surfaces of the six emitters (Re) forming a cylindrical cavity of 0.61-inch radius and 0.658-inch length. The front opening of the cavity is to be placed at a distance of about 0.4 inch behind the mirror's focal plane, i.e., towards the sun. This produces optimum impingement and absorption of the solar energy on the cavity wall. A tungsten cone with a 1-inch diameter opening protects the cavity walls from adverse effects caused by misalignment of the generator and the mirror. The rear of the cavity is formed by a highly reflective electropolished W surface (rear piece) in the form of an inverted, doubly truncated cone, so designed as to direct reflected solar energy uniformly to the cavity wall (the emitters). This rear piece reflector is thermally isolated from the converters. The energy absorbed by the reflector is dissipated by a large Cr_2O_3-coated Mo radiator which is brazed to the W piece by a high temperature braze. During solar operation the W rear piece is designed to operate at a temperature less than 1200°C. With this solar image-cavity arrangement, which is expected to result in a near-optimum generator performance, approximately 4500 watts of solar energy enter the cavity; 200 watts are absorbed by the front piece; 2300 watts are absorbed by the six Re emitters; 1400 watts are absorbed

by the W back piece; the remaining 600 watts are reflected and/or re-radiated and escape through the front opening of of the cavity.

2. In the fabrication of the various parts of the JG-4 and final assembly of the unit, considerable effort was expended in the preparation of the Re sleeves, which developed vacuum leaks during machining or thermal cycling. These leaks resulted from voids left in the seam of the Re tubing during the heliarc-welding process conducted by the vendor. This problem was eliminated after the Re tubing was purchased from the vendor in the "rolled only" state and the seam was electron-beam-welded by TECO. Substantial effort was also expended in the fabrication of the emitters which, due to their complex geometry and extremely close tolerances, required special preparatory techniques, particularly during electron discharge machining and subsequent processing. Finally, considerable effort was devoted to the generator assembly, which required the fabrication of special tools for aligning to critical tolerances the converters and the back-piece which form the cavity. Prior to constructing the Mo block, to which the various parts of the gnerator were mounted, an Al model was fabricated and checked for feasibility of the overall block design.

3. Twelve identical thermionic converters were fabricated and individually tested; six of these converters were mounted on the generator. During the test of each converter, the output current was measured at different

output voltages and at given emitter temperatures, with the cesium temperature optimized for maximum output. All twelve converters generated nearly identical data of the following typical values:

Output Voltage = 0.7 volt
Output Current = 53.5 amperes
Emitter (Hohlraum) Temperature = 2000°K
Cesium Temperature = 630°K
Collector Temperature = 1045°K

The above current-voltage data indicate an average power output of 37.5 watts from each converter, or a total of 224 watts from the six converters. The same power output was obtained at a lower emitter temperature but also at a lower output voltage.

4. Other work performed in association with the JG-4 included the evaluation of the thermal transfer characteristics of the 0.65 Pd - 0.35 Co braze selected for joining the W and Mo parts of the cavity back-piece. For this purpose two samples, identical in geometry, were prepared and tested. One sample consisted of a W and a Mo disk joined together with the 0.65 Pd - 0.35 Co braze; the other sample was a solid Mo disk. Both samples were tested under identical conditions and comparison of the test results indicated that the rate of heat transfer in the W-braze-Mo sample was equal to or slightly higher than that measured in the all-Mo sample.

5. For laboratory tests of the JG-4, an electron bombardment unit was fabricated and tested. This unit consisted of six hairpin W filaments arranged to form a cylindrical unit suitable for insertion into and heating of the generator cavity. The W filaments could be connected either in parallel, and controlled as a single unit, or individually, and controlled as six separate units. The unit was tested inside a cylindrical Mo block having approximately the same geometry as the generator cavity. The test results indicated that for a temperature of about 2000°K on the Mo surface facing the filaments, a total output power of 2200 watts was required from the filament assembly.

CHAPTER 2

GENERATOR DESIGN

The original design of the six-converter solar thermionic generator (JG-4) is discussed in detail in the TECO Report No. TE18-66. This design provided for Re emitters pressure-bonded to a Ta substrate and Ta sleeves in the converters and also for Ta shoe-pieces in the generator cavity. The cavity, of hexagonal cross section, was to be formed by the rear surfaces of the emitters and "shoe-pieces" which were to be welded to the emitters. These "shoe-pieces" were to be perpendicular to the emitters in the rear of the cavity. Most of the solar energy reaching the rear of the cavity was to be intercepted by the six "shoe-pieces" and transferred to the emitter surfaces primarily by conduction with some radiation. The front cavity surface is open to admit the solar energy.

Prior to the fabrication of the JG-4 a detailed review of its design was performed with particular emphasis on the emitter and sleeve materials and the cavity geometry. This review was prompted by recent converter life test results at JPL which indicated that converters employing Ta sleeves and pressure-bonded Re emitters often failed after an extended period of operation due to the following reasons:

1. When the converter operated in a horizontal position, the sleeve sagged, causing an electric short between emitter and collector.

2. The sleeve developed a leak at its hottest region, near the emitter, due to prolonged attack by residual gases (e.g. O_2) present in the converter test environment (vacuum of about 10^{-5} - 10^{-6} torr).

3. The life tests of the converters revealed a reaction between the Re emitter and the Ta substrate to which it was pressure-bonded, resulting in an inter-diffusion of the two metals at their interface and the formation of Kirkendall holes. This, in turn, caused a partial separation of the metals with a resultant shorting of emitter to collector as well as a reduction in the thermal conductivity of the composite emitter due to the porosity of the Kirkendall holes.

Converters using Re sleeves and solid Re emitters did not develop the above adverse effects because of the high mechanical strength and the chemical inertness of the Rhenium and the elimination of the Ta substrate.

In view of the above results it was decided to change the pressure-bonded Ta-Re emitter and the Ta sleeve in the converters of the JG-4 generator to Rhenium. This change, because of the low thermal conductivity of Re compared to Ta, made the "shoe-piece" concept unacceptable. The temperature gradients in the emitters and the "shoe-pieces" would have been too large. It was necessary to change the cavity geometry so that the emitter temperature distribution was controlled by radiation transfer r r than conduction transfer. This was accomplished by replacing the "shoe-pieces" with a highly reflective element in the rear of the cavity (back piece) so designed as to direct most of the solar energy incident on it back to emitters by reflection. The back-piece, in the form of a doubly truncated inverted cone, covers the whole rear opening of the cavity and is both thermally isolated and electrically insulated from the emitters.

Also in order to enhance the uniformity of temperature distribution in the emitters, their rear surfaces, which form the peripheral part of the cavity, were designed to form a cylindrical wall instead of a hexagonal one as originally intended. To provide for a smaller temperature gradient through the emitter thickness, this dimension was reduced in the new design; the higher mechanical strength of Re over Ta allowed for this reduction. Finally, to increase the absorptivity of the emitter rear surfaces in the cavity, these surfaces were designed with grooves cut parallel to the cavity axis. (Described in the text following and illustrated in Figure 4.) The replacement of the conductive Ta "shoe-pieces" by a reflective electropolished W back-piece was prompted also by the lack of confidence on the heat transfer capability of the weld between the "shoe-piece" and the emitter. A poor weld would have cause the "shoe-piece" to attain prohibitively high temperatures that could result in catastrophic failure of the generator. Furthermore, the welding of a "shoe-piece" to an emitter was to be performed after the emitter was incorporated into a converter. This operation presented severe problems associated with the critical alignment of the "shoe-piece" and the structural integrity of the emitter.

Based on the original data supplied by JPL, taking into consideration the mirror geometry and the pseudo-source of solar energy, (a point-source solar image) a new cavity design was prepared. A detailed study (Appendix A) was performed on the heat transfer mechanisms of the radiant energy in the cavity and the optimization of the flux distribution. Following this study additional and more accurate information about the mirror geometry, the solar image

and the energy distribution at the focal plane was supplied later by JPL. Further investigation on the optimum cavity design was conducted, and the results of this work are presented in Appendix B. Data regarding the geometry, physical properties and operational characteristics of the final JG-4 cavity assembly, including the converters, are summarized below. These data are based on the design analyses presented in Appendices A and B and on experimental results obtained in previous related programs.

The final JG-4 cavity is in the form of a cylinder of 1.22-inch diameter with its axis coincident with the optical axis (the normal to the apex of the mirror). The peripheral surface of the cavity is formed by the rear surfaces of the six Re emitters spaced 0.024 inch from each other; each surface is 0.658 inch long and is grooved along this dimension with 29 parallel rectangular grooves each 0.010 inch wide and about 0.020 inch deep. This type of surface increases the absorptivity of the Re surface to about 0.75. A cylindrical hole, 0.020 inch wide, 0.160 inch deep, for pyrometric temperature measurements, is centrally located on the side facing the mirror in each of the emitters. The center of the hole is 0.040 inch away from the rear surface and 0.070 inch away from the front surface of the emitter. The estimated temperature difference along the 0.070-inch path is about 40°K when the thermionic surface of the emitter is near 2000°K (the rear at about 2070°K). The current from emitter to collector is about 60 amperes and the output voltage is 0.7 volt, resulting in a converter power output of 42 watts. This output occurs at an estimated emitter-collector separation of 2 mils, and corresponds to a collector temperature of about 1030°K and a cesium reservoir temperature of about 630°K.

The heat losses from the emitter, neglecting heat conduction through the sleeve, are approximately 230 watts. The cylindrical Re sleeve is 5 mils thick, 0.48 inch long and has an inside diameter of 0.64 inch. The heat conduction loss through the sleeve is about 20 watts for a temperature gradient of 900°K along the length of the sleeve, assuming perfect shielding for radiation losses.

The sleeve shield consists of a minimum of five Ta cylinders, 5 mils apart from each other, formed by a continuous wrap of Ta sheet 0.001 inch thick. Assuming that the average temperature of the sleeve is about 1500°K, that the Ta emissivity is 0.2, and neglecting any radiation exchange between sleeve and collector, the total radiation loss from the sleeve of 1 $in.^2$ lateral area is about 5 watts. An additional Re shield in the form of a flat square with a circular hole to allow for the cylindrical (0.658 in. dia) emitter body is placed behind the exposed four flat corners (total area 0.09 $in.^2$) of the rear part of the emitter to reduce radiation losses: again, as with the sleeve shield, the losses through this shield are negligible.

The front opening of the cavity (nearer the mirror) is formed by the front-piece, having a 1-inch diameter circular aperture centered at the cavity axis and located 0.11 inch away from the edge of the cavity wall (the emitter rear surfaces). The front-piece, thermally isolated from the emitters, is made of W and its surface, facing the mirror, is in the form of a cone inclined at an angle of 52° with the optical axis. This polished surface has an area of about 18.6 $in.^2$, and is maintained at an average temperature of about 1000°K when the solar energy incident on this surface is about 200 watts. The total emissivity and the total reflectivity of polished W at 1000°K are

approximately 0.11 and 0.55, respectively. Radiation exchange between the front-piece and the six converters is assumed to be negligible. The difference between their average temperatures is small and five radiation shields are placed on the back of the front pieces (front cone).

The rear opening of the cavity is occupied by the back-piece, which is symmetrically located about the cavity axis, and is thermally isolated from the converters. This piece consists of two parts; (1) the front, made of W, which serves as a reflector of the solar energy and (2) the rear, made of Mo, which serves as a radiator for the absorbed solar energy. The surface of the front part, facing the cavity, is in the form of a doubly truncated cone, designed so that the major portion of the reflected solar energy is uniformly directed toward the six emitters. The top opening of this surface is placed 0.12 inch away from the edge of the emitters. The electropolished surface has an area of about 1.86 $in.^2$ and during solar testing will be at a temperature of about 1200°K. This temperature is controlled by the radiation loss from the rear part surface, which is grooved and Cr_2O_3-coated to produce a total emissivity of at least 0.75. It has a 76-$in.^2$ area and is capable of dissipating 1800 watts when its average temperature is approximately 950°K. The geometry and the temperature distribution of the rear part of the back-piece are discussed in Appendix C.

The rear and front parts of the back-piece are joined together by a high temperature braze, (0.65 Pd-0.35 Co). The thermal resistance of this braze, measured across a W/0.65 Pd-0.35 Co/Mo disk in a specially designed experiment, was found to be equal to or

less than the thermal resistance of an all-Mo disk of equal cross-section and thickness. Details of this experiment are given in Appendix C. The energy radiated from the back-piece is absorbed mainly by water-cooled copper heat sinks that surround the radiating surfaces. The absorbing surfaces of the heat sinks are Cr_2O_3-coated. The heat sink also serves as the generator support structure and has provisions for terminating all the instrumentation wires extended from the converter and other parts of the generator.

The design of the back-piece, in particular the tungsten front part, depends upon the assumed energy distribution within the cavity. The present design of this piece is based on the most recent data supplied by JPL regarding the geometry of the mirror, the size of the solar image and its energy distribution, and also the variation of the solar energy distribution in the cavity with image position. The details of the design are presented in Appendices A and B, which deal in detail with the design parameters of the cavity and particularly of the back-piece. The results of these studies indicate that the near-optimum mirror-cavity arrangement requires a cavity front-solar image separation of about 0.4 in. with the image located on the axis of the cylindrical cavity. In this arrangement a total amount of 4500 watts of solar energy enter the cavity; 200 watts are absorbed by the front-piece; approximately 2300 watts are absorbed by the six emitters, while approximately 1400 watts are absorbed by the back-piece; the remaining 600 watts are reflected and/or re-radiated and escape through the front opening of the cavity.

CHAPTER 3

GENERATOR FABRICATION

Following completion of the JG-4 design, the fabrication and assembly of the generator was performed in several stages including: 1) fabrication of the generator frame (block); 2) fabrication and assembly of twelve identical thermionic converters (six mounted in the generator); 3) fabrication of other parts of the generator, e.g., the front-piece, back-piece, supports, etc.; 4) fabrication of the back-piece radiator and the cooling jacket-generator support, including thermocouple terminations; 5) fabrication and assembly of a multi-filament electron-bombardment gun; and 6) assembly of the generator.

Prior to the fabrication of the molybdenum generator frame, an aluminum model was made and used for checking structural details and assembly tolerances. The final frame, with the cavity back-piece, radiator, frame support structures, and front-piece mounted in place, is shown in Figure 1. The grooved and Cr_2O_3-coated molybdenum rear surface (radiator) of the back-piece and the polished tungsten front-piece are clearly shown in this figure. Details of the converter mounting provisions and the thermocouples (chromel-alumel) used for monitoring the frame's temperature can also be seen in the same figure. Figure 2 shows the frame mounted on the copper cooling jacket; the holes in the jacket are for mounting terminal posts for the thermocouples, cesium heater leads, and voltage probes used in the generator operation.

A typical thermionic converter used in the JG-4 generator is shown in Figure 3. The grooved and Cr_2O_3-coated copper radiator, the copper tube cesium reservoir, its heater (platinum) and heat shield

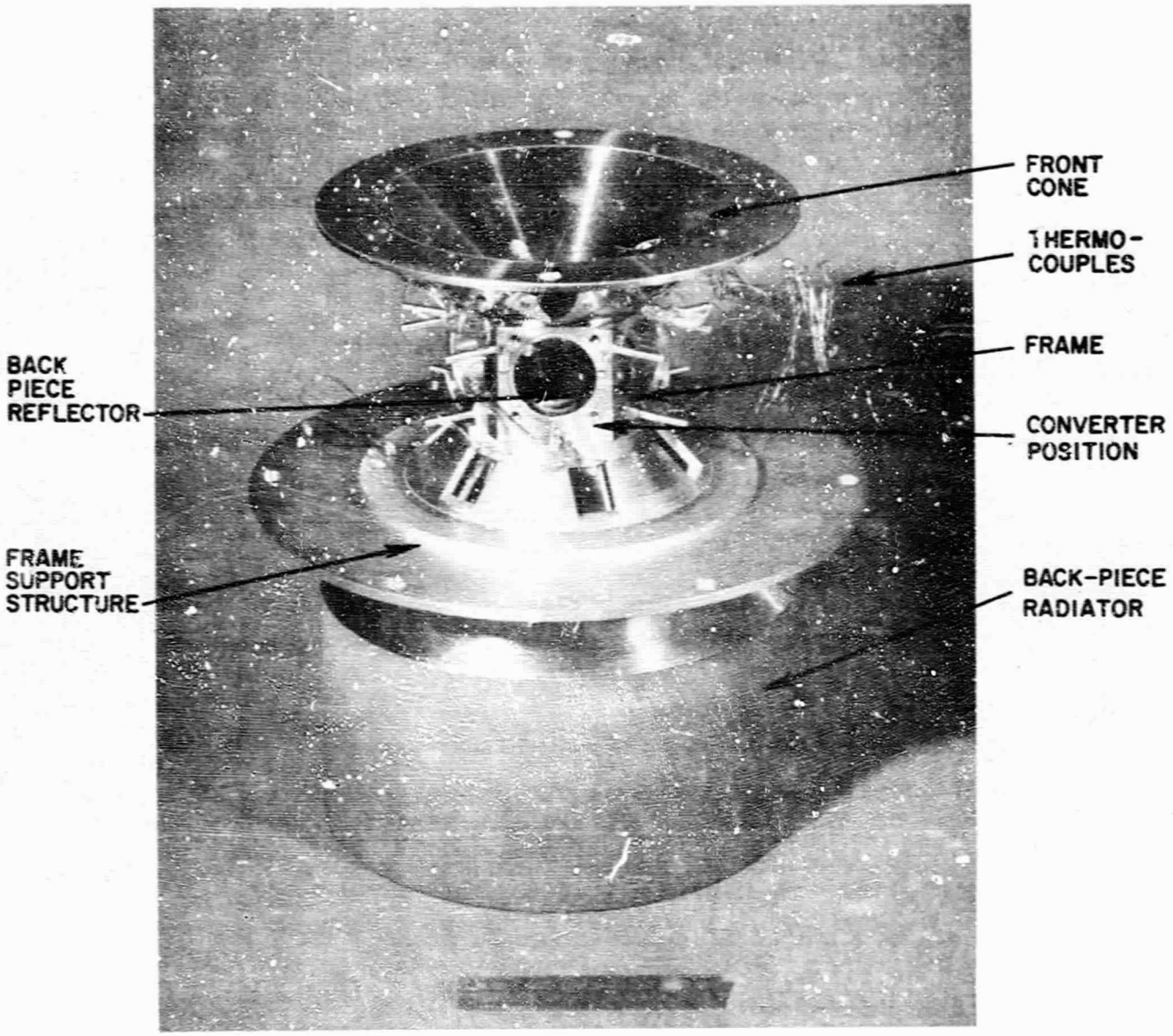

Figure 1. JG-4 Frame with Cavity Front an: Mounted in Place.

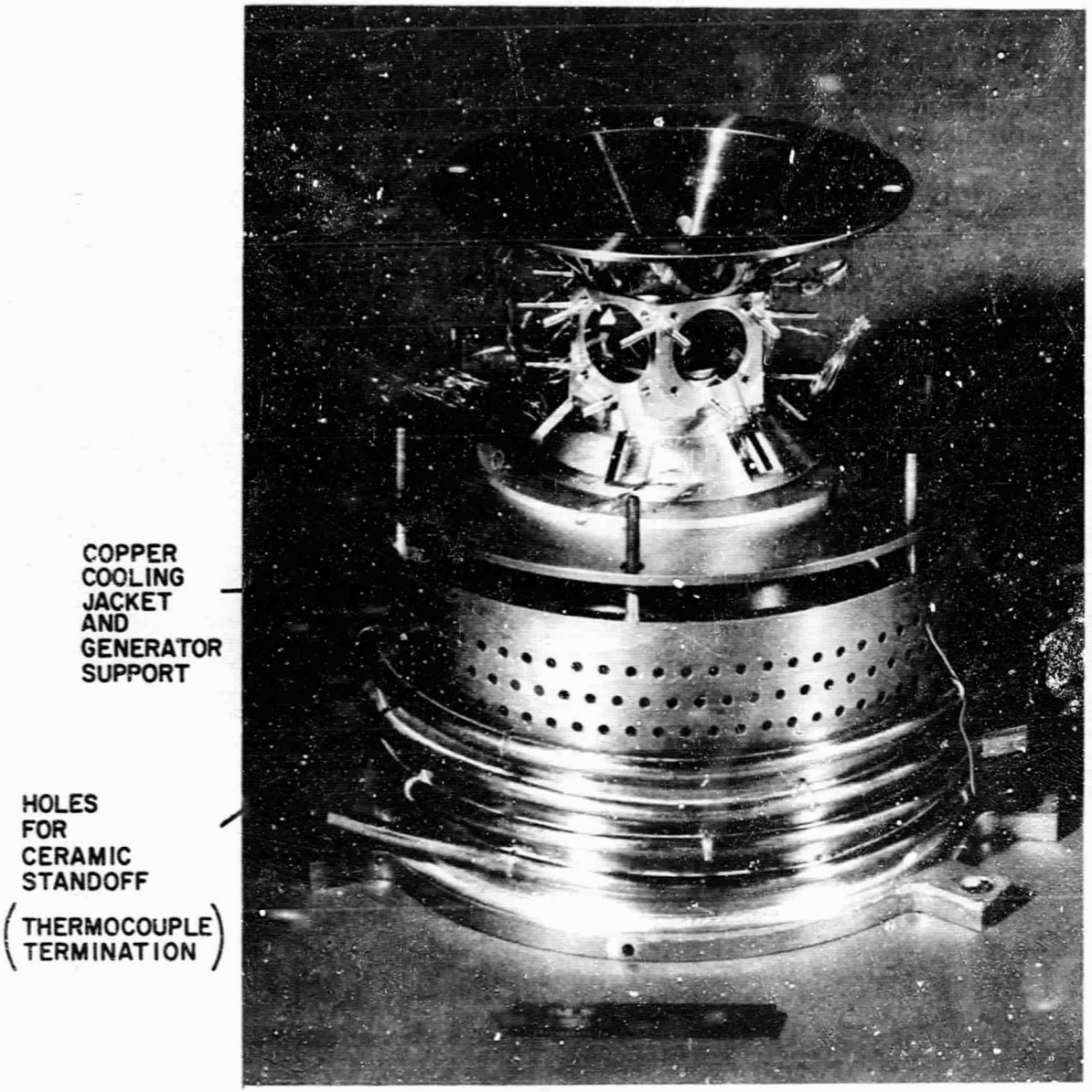

Figure 2. JG-4 Frame with Back Piece Surrounded by Cooling Jacket.

(nickel) and the niobium-Al_3O_3 emitter-collector seal are clearly shown in this figure. The tantalum support for the multi-layer radiation shield around the sleeve and part of the emitter including the hole for pyrometer temperature measurement are also shown in this figure. The chromel-alumel thermocouples used for monitoring the temperature of the various parts (e.g., collector, radiator, cesium reservoir) of each converter are also evident in Figure 3.

A detailed view of the rhenium emitter used in the converters of the JG-4 is shown in Figure 4. Both the flat, smooth front (facing the collector) and the cylindrical, grooved rear (part of the cavity) surfaces of the emitter are clearly shown. The generator cavity is shown in detail in Figure 5 where the six converters used in the JG-4 are shown mounted on the frame. In this figure the electropolished tungsten front surface (reflector) of the back-piece is in clear view.

The six-filament electron-bombardment assembly used for preliminary tests of the JG-4 is shown in Figure 6. The filaments (tungsten) share a common heat reflector (rhenium) centrally mounted at the top of the assembly.

The complete JG-4 generator is shown in Figures 7 and 8 (less front-piece). Figure 8 also includes the electron-bombardment gun, mounted on the front-piece of the generator. In this figure, the two heavy posts (copper) shown on the side of the generator are the emitter and collector current leads of the six converters, connected in series.

During fabrication of the generator, extensive effort was expended in the fabrication of the rhenium emitters and sleeves.

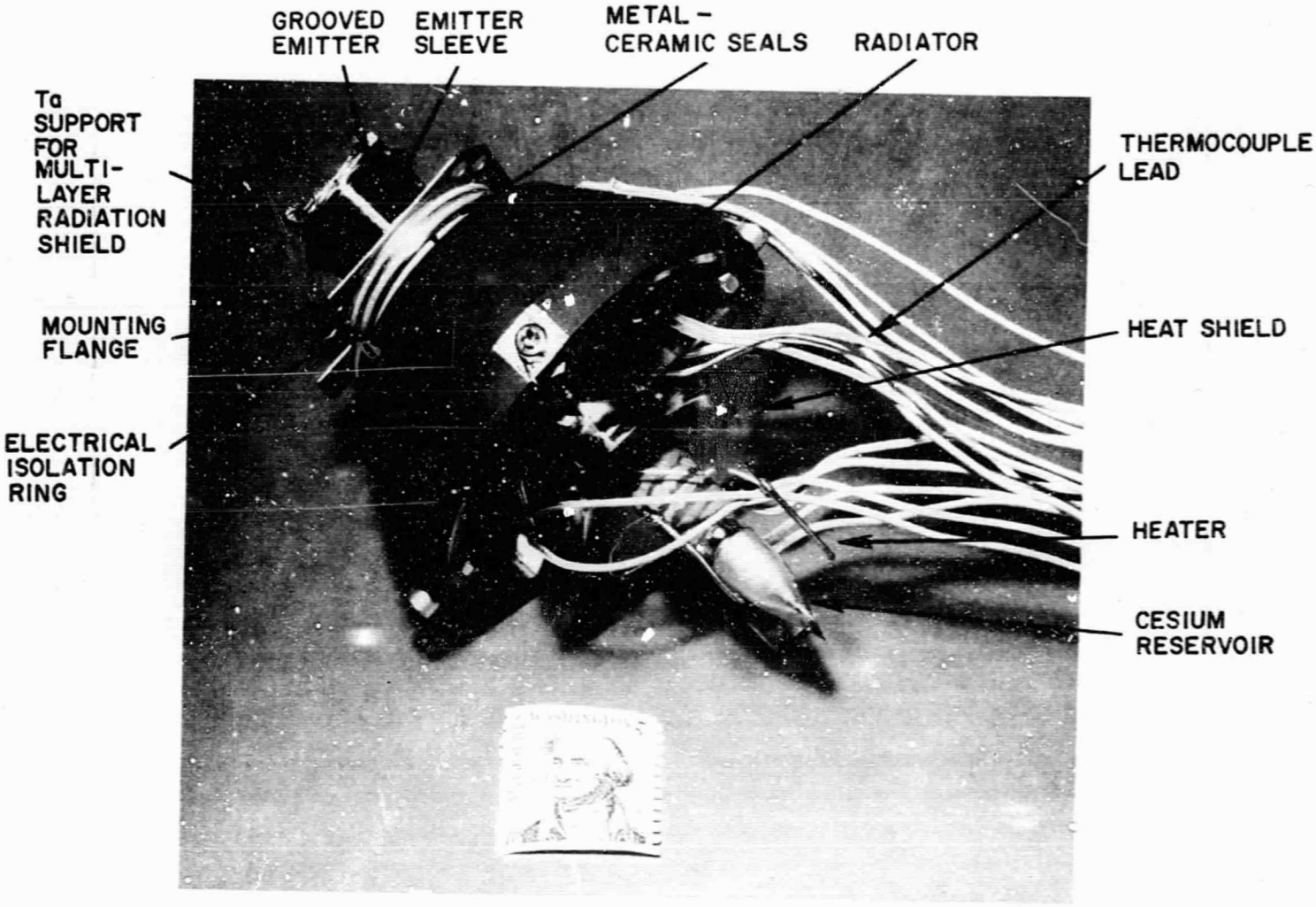

Figure 3. Typical Thermionic Converter used in JG-4.

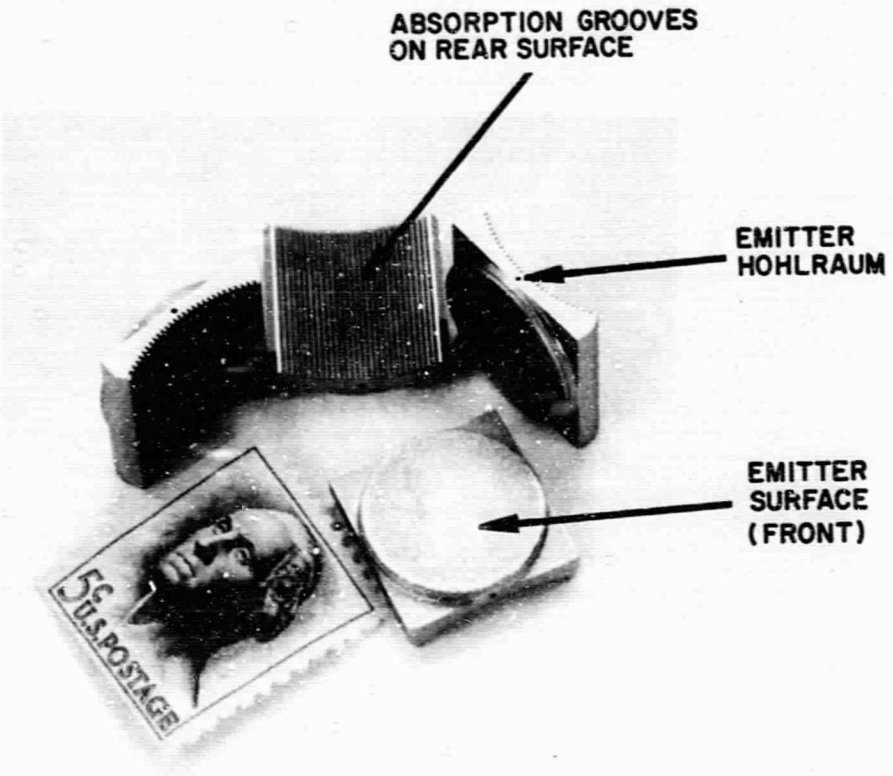

Figure 4. Rhenium Emitter used in JG-4 Thermionic Converters.

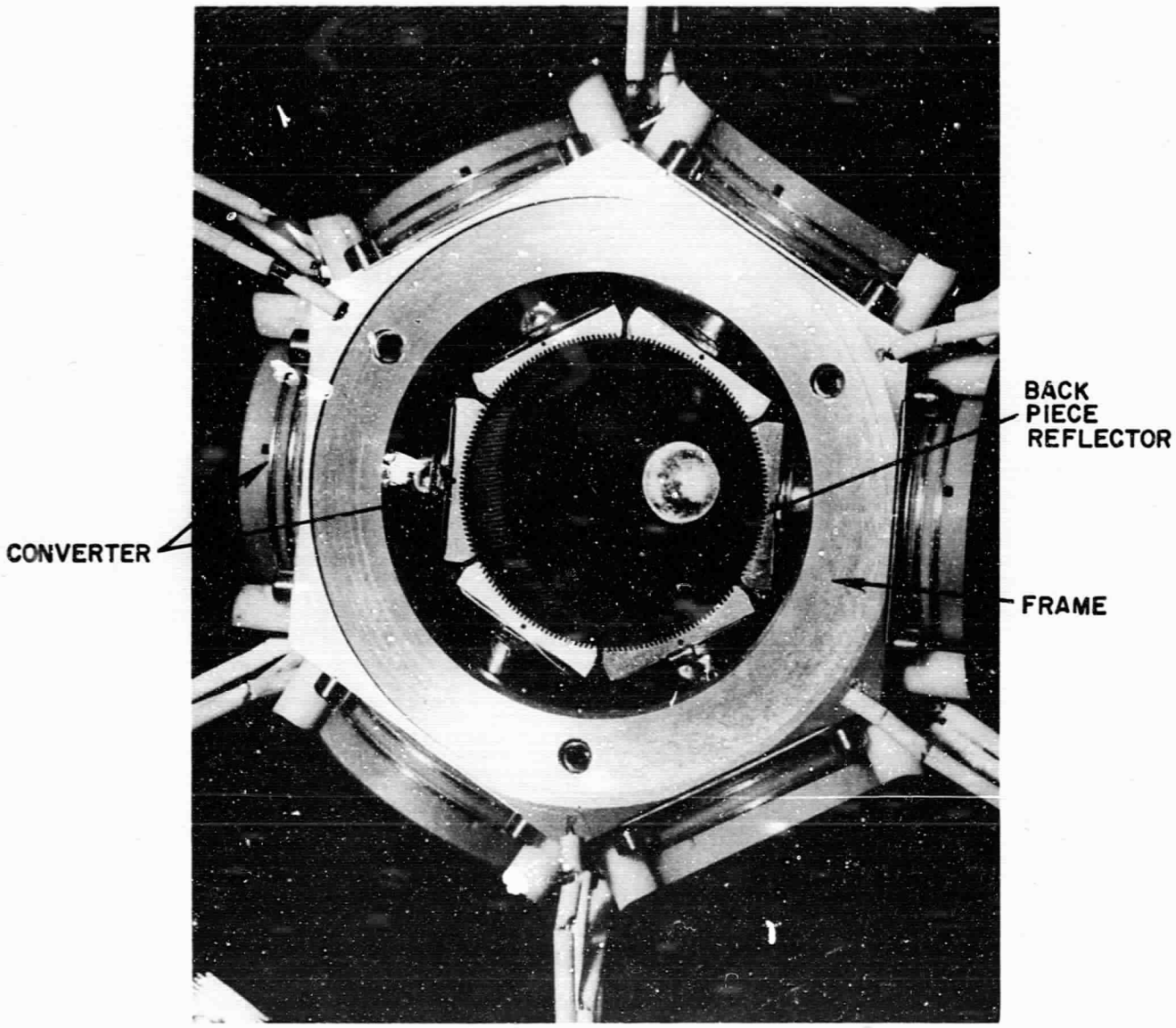

Figure 5. JG-4 Cavity.

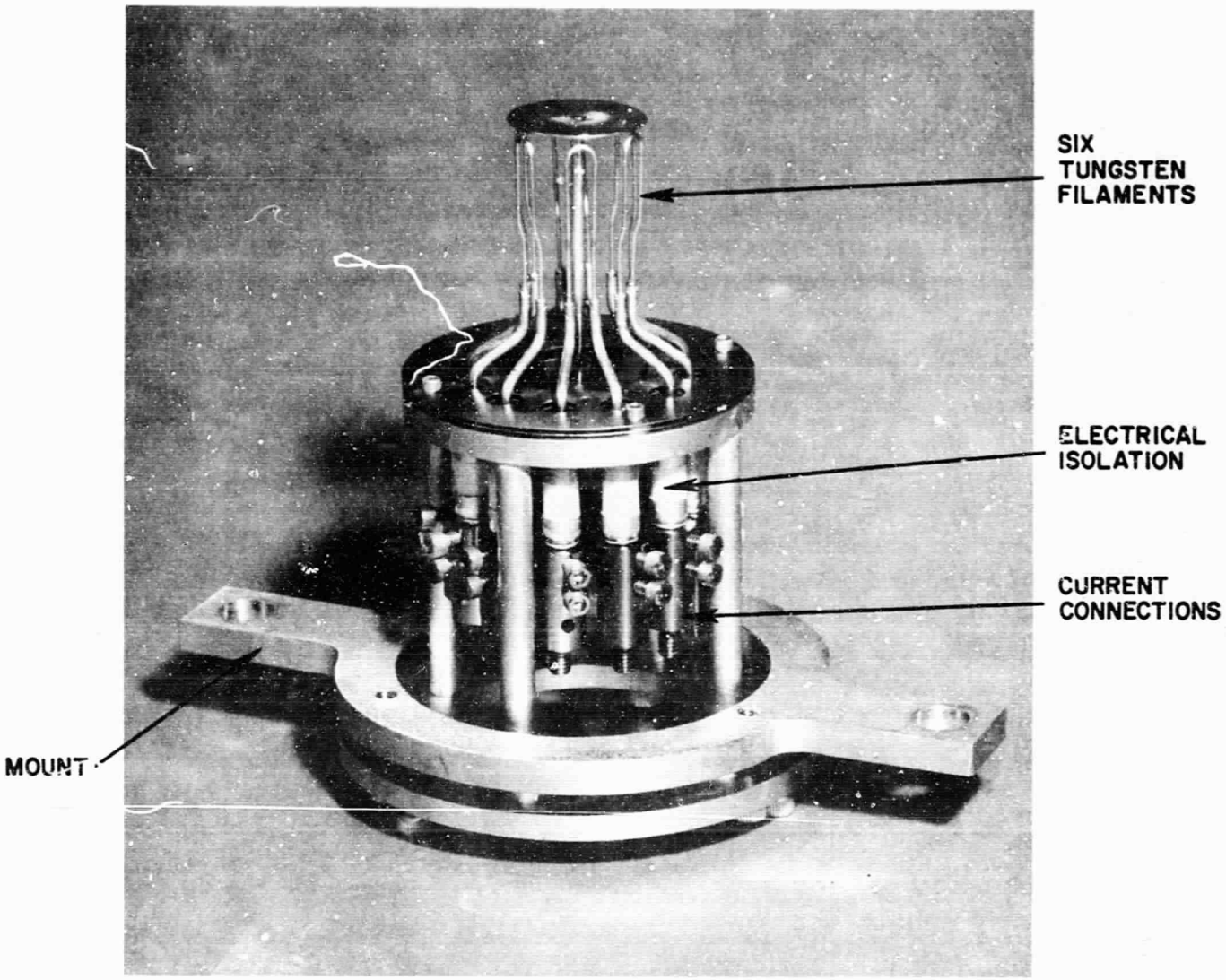

Figure 6. Electron-Bombardment Gun used for Laboratory Test of JG-4.

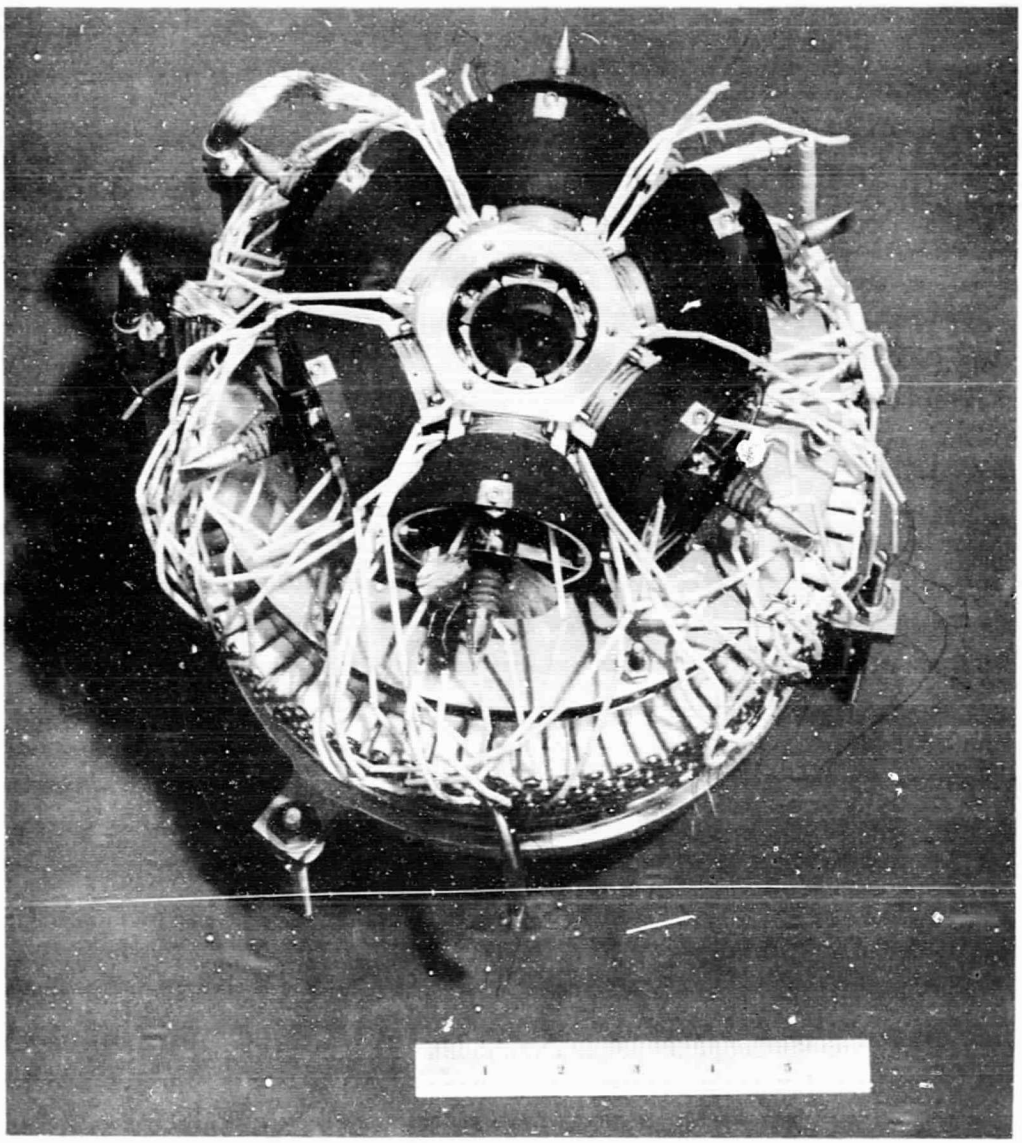

Figure 7. Complete JG-4 (Less Front-Piece).

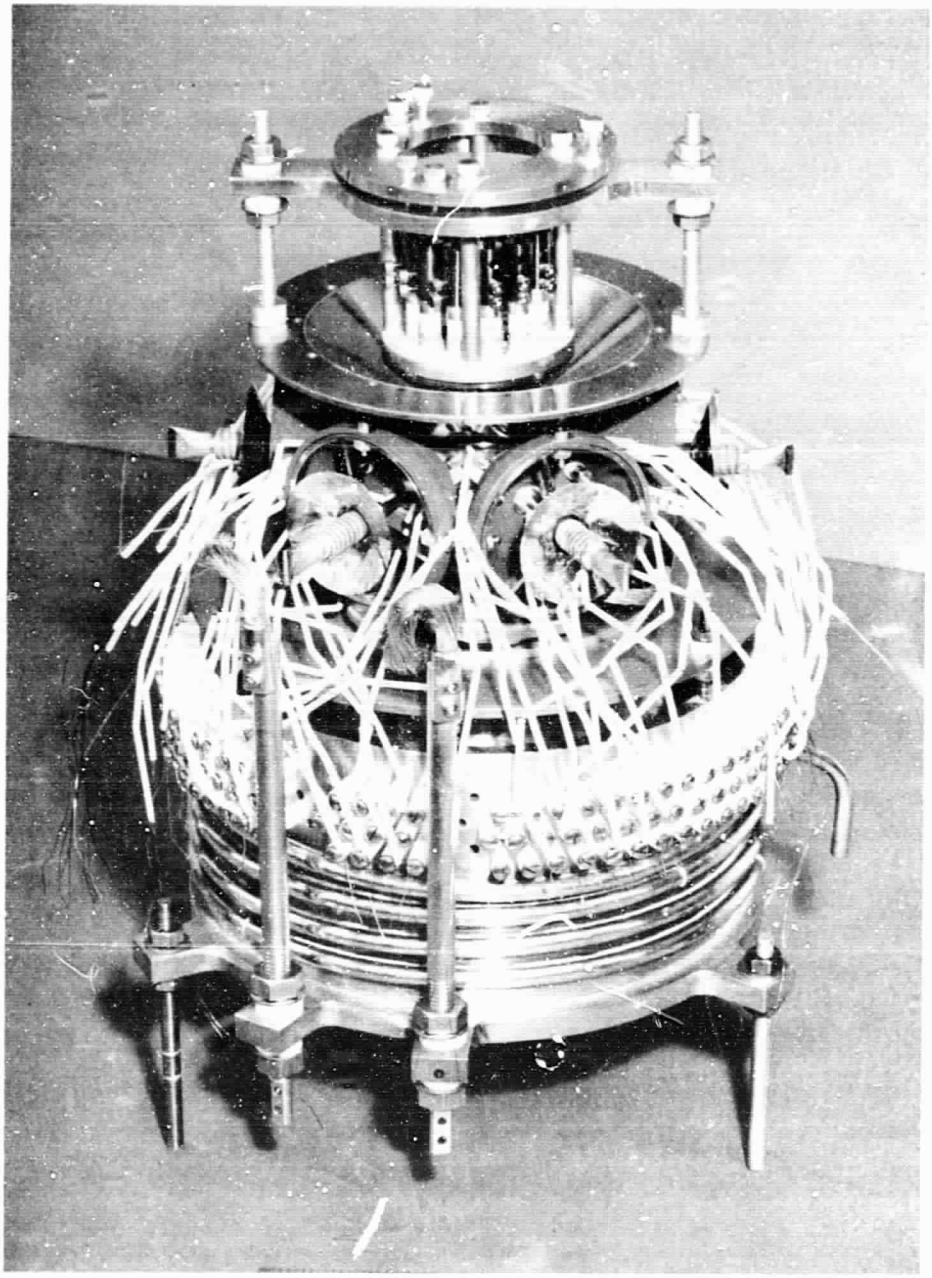

Figure 8. Complete JG-4 with Electron-Bombardment Unit.

Because of their complex geometry and close tolerances, the emitters required special manufacturing procedures, particularly during the electron-discharge machining (EDM) of their grooved cylindrical surfaces. The rhenium sleeves, of 5-mil wall thickness, also required special methods for their construction due to the problem of maintaining structural integrity, particularly at the sleeve's seam during the thermal cycling of a sleeve performed prior to incorporating it into a converter. Forming of the seam of a sleeve was accomplished by electron-beam welding; the same method was also used for joining the sleeve to the niobium flange of the emitter-collector seal and the sleeve to the emitter. Because of some difficulties encountered in this operation, the last six converters, out of a total of twelve built for this program, had their sleeves joined to the seals with vanadium brazes. Considerable care and effort were also devoted to assembling the generator, with particular emphasis on the cavity area, where very small tolerances and critical alignment were required.

CHAPTER 4

CONVERTER TESTS

All converters built for this program had identical overall configuration employing planar electrode geometry with polycrystalline rhenium emitters and molybdenum collectors. The effective area of the emitter and the interelectrode spacing were estimated to be 2 cm^2 and 0.005 cm, respectively, during converter operation. Twelve converters were completed for this program; six of these were mounted on the frame of the JG-4 generator. All converters were subjected to identical performance tests using a static load between emitter and collector. Each converter was tested at an emitter temperature of 1975°K for output voltages of 0.6, 0.8, 1.0 and 1.2 volt, and at 2000°K for 0.7 volt. During test the cesium temperature was optimized for maximum output current at the given voltage. The collector temperature was not controlled independently but it depended on the emitter and cesium temperatures and varied within a range determined by the heat rejection rate afforded by the converter design. The emitter was heated by an electron-bombardment gun placed near the exposed flat surface of the emitter. A 1000-volt potential was applied between the gun and the emitter. The cesium temperature was controlled by a platinum wire heater surrounding the cesium reservoir.

In all tests the emitter temperature was measured by an optical pyrometer through a hole in the emitter body. This temperature was corrected for pyrometric errors and for absorption loss in the glass wall of the bell jar surrounding the converter. All converters were tested in a vacuum of about 2×10^{-6} torr. The collector and cesium

temperatures as well as the temperature of other parts of the converter (e.g., radiator, seal, etc.) were monitored by chromel-alumel thermocouples mounted on the converter. Multi-foil thermal shielding of the sleeve was not used in these tests.

The performance of converters Nos. 3, 4, 5, 10, 14 and 15 is shown in Figure 9, where the output current (I) is plotted versus the output voltage (V); the collector (T_C) and cesium (T_R) temperatures are also plotted in the same figure. These six converters, after test, were used in the JG-4 generator. The performance of the other six (spare) converters, Nos. 2, 7, 8, 9, 12 and 16 is shown in Figure 10, where again I, T_C and T_R are plotted versus V. These tests were performed at an emitter temperature (T_E) of 1975°K. Table I shows the output current, output power and the value of T_R and T_C for each converter at V = 0.7 volt and at T_E = 2000°K. It can be seen from this table that the average output power of all converters tested is 37.5 watts obtained at average collector and cesium temperatures of 1045°K and 630°K, respectively.

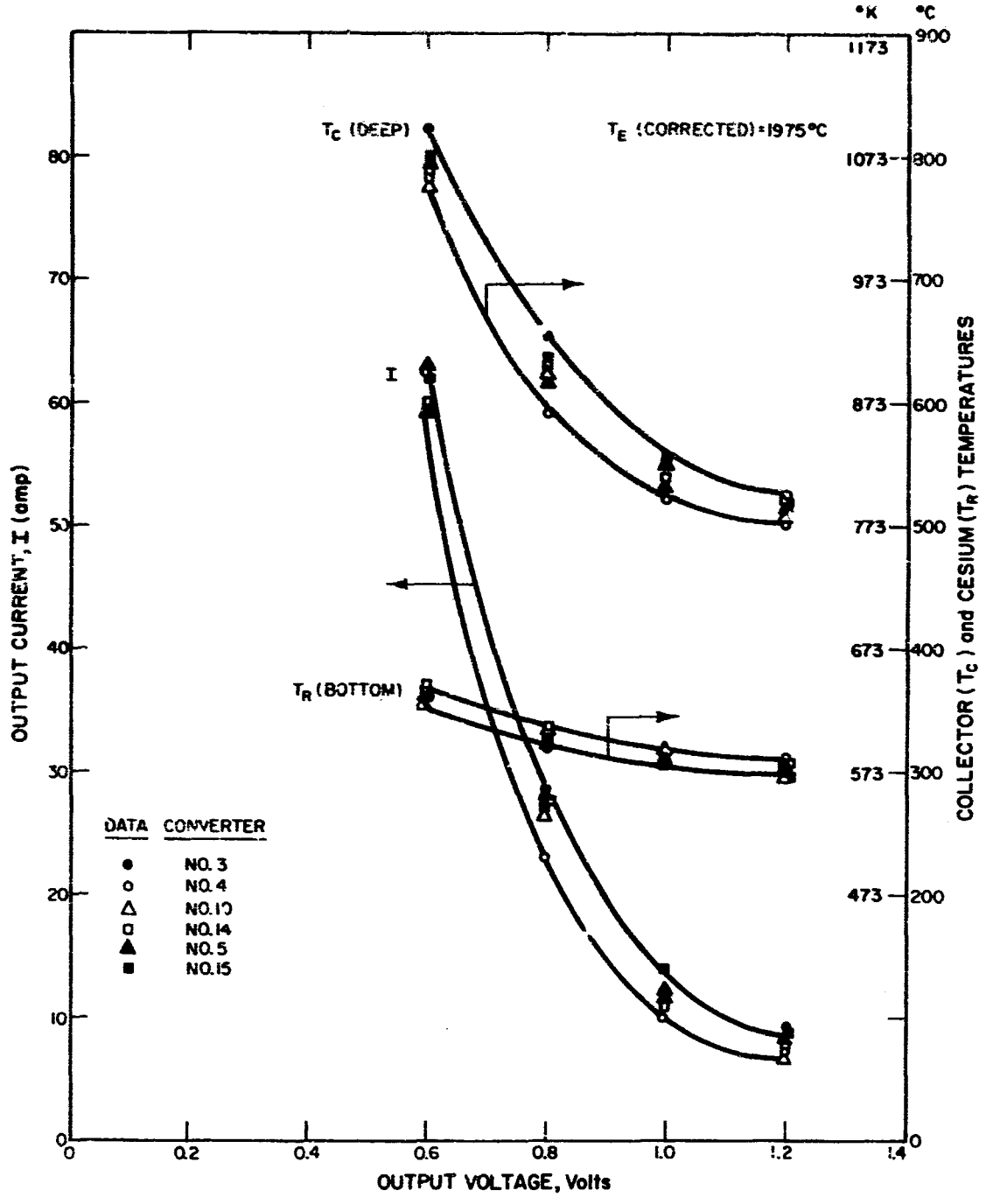

Figure 9. Performance Characteristics of Six Converters Used in JG-4.

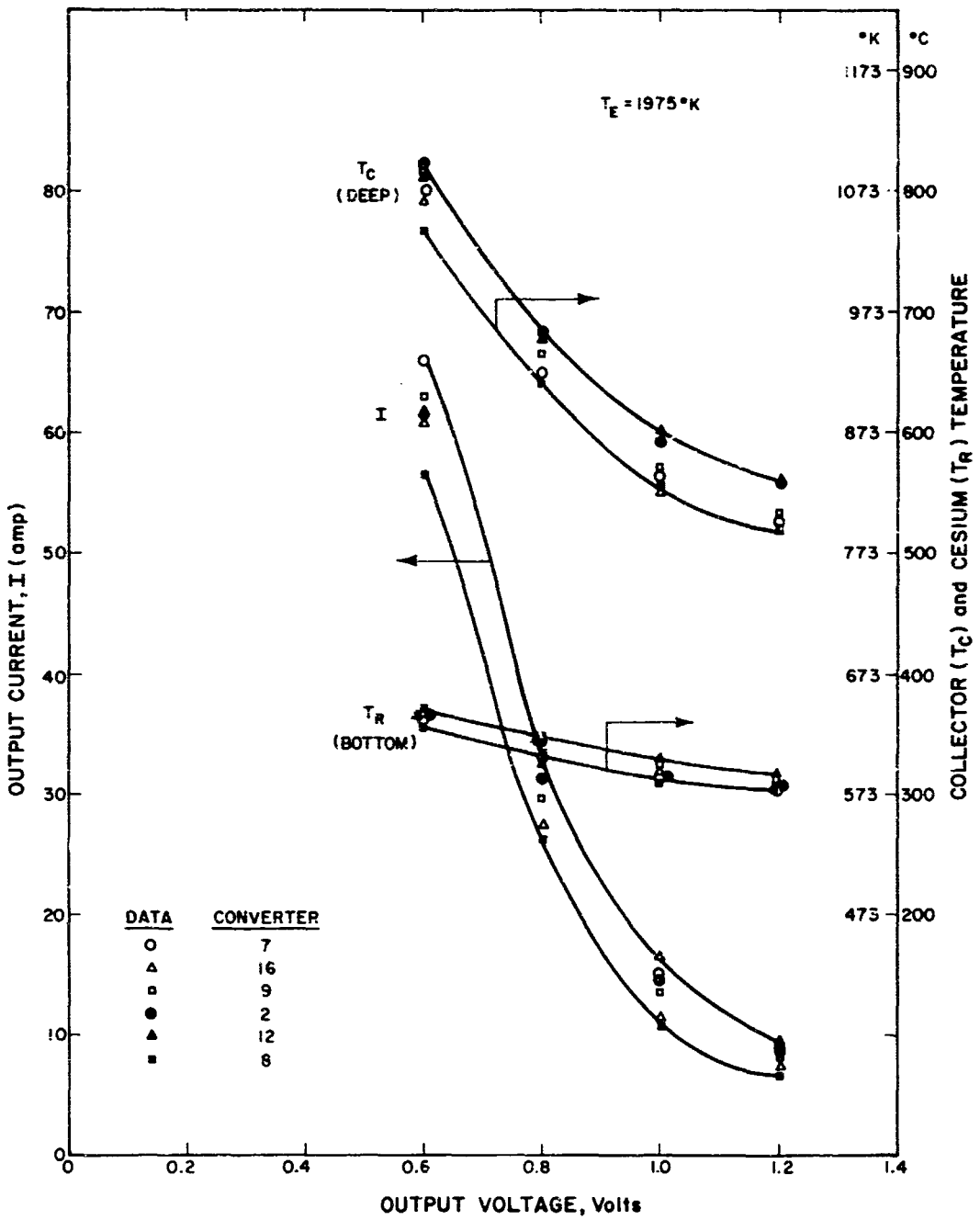

Figure 10. Performance Characteristics of Six Spare Converters.

TABLE I

CONVERTER OUTPUT CURRENT AND POWER

(Output Voltage = 0.7 volt; Emitter Temperature = 2000°K)

	Converter No.	Output Current (amp)	Output Power (watt)	Collector Temperature (°K)	Cesium Temperature (°K)
Mounted in JG-4	3	55.0	38.5	1075	622
	4	54.0	37.8	1031	628
	5	54.0	37.8	1036	626
	10	52.0	36.4	1031	626
	14	52.5	36.8	1027	627
	15	53.0	37.1	1032	623
	Average	53.4	37.4	1039	625
Spares	2	53.0	37.1	1066	633
	7	58.0	40.6	1047	640
	8	50.0	35.0	1035	628
	9	54.0	37.8	1061	636
	12	54.5	38.2	1056	630
	16	52.5	36.8	1038	637
	Average	53.7	37.6	1051	634
	Average (12 converters)		37.5	1045	630

CHAPTER 5

ELECTRON-BOMBARDMENT UNIT

An electron-bombardment gun was constructed for laboratory test of the JG-4 generator. The gun consists of six identical hairpin tungsten filaments mounted on tantalum posts terminating in a molybdenum flange through Al_2O_3 electrical insulators. The filaments are arranged in a cylindrical configuration suitable for the cavity of the JG-4 generator. Tantalum and rhenium heat shields are used at the front and rear of the filament assembly. The complete unit is shown in the photograph of Figure 6.

The unit was tested inside a molybdenum cylinder having approximately the same geometry as the cavity of the JG-4. Both the inside and outside surfaces of the cylinder were grooved, and a hole for pyrometric temperature measurements was provided on the cylinder wall. During this test, the filaments, connected in series, were heated up to about 2300°K with an input power of 845 watts (32.5 amperes, current), provided by an ac supply. An electron accelerating potential of 1000 volts was applied between the filaments and the molybdenum cylinder, which received an electron-bombardment power of 2200 watts; part of this power was dissipated by radiation from two molybdenum disks attached to the ends of the cylinder. During this test, the cylinder's inner surface, facing the filaments, reached a temperature of approximately 2000°K, while the average temperature of each filament was 2300°K. After test the electron-bombardment unit was mounted on the JG-4 generator as shown in the photograph of Figure 8.

APPENDIX A

REVIEW OF THE DESIGN DATA FOR THE CAVITY OF THE JG-4

CAVITY DESIGN

1. SOLAR SOURCE

The cavity temperature depends on the intensity of the solar flux at the sun's image formed by the mirror in front of the cavity. For a parabolic mirror the sun's image formed at the focal point of the mirror from a beam of rays reflected from a single point on the mirror has an elliptical cross section of semi-axes a and b, (see Figure A-1). (The sun's image formed by rays reflected from all points on the mirror has a circular cross section of radius a.) The focal length (f) of the mirror is:

$$f = \frac{R_m (1 + \cos \theta_m)}{2 \sin \theta_m} \qquad \text{(A-1)}$$

where R_m and θ_m are the rim radius and angle of the mirror respectively. The semi-axes a and b are:

$$a = \frac{\psi R_m}{\sin 2 \theta_m} \qquad \text{(A-2)}$$

and

$$b = \frac{\psi R_m}{2 \sin \theta_m} \qquad \text{(A-3)}$$

The cross section of the sun's image is simply

$$A_s = \pi a^2 \qquad \text{(A-4)}$$

In the above equation $\psi = 0.0093$ rad. [The solar angle is 32']. For a parabolic mirror having $R_m = 57"$ and $\theta_m = 45°$ the above equations

result in: f = 69", a = .530", b = 0.375" and A_s = 0.885 in.^{2}. The solar energy (W) at the focal point of the mirror is:

$$W = \pi C f^2 \sin^2 \theta_m \tag{A-5}$$

where

$$C = \frac{\psi^2}{4} \sigma T_s^4 \tag{A-6}$$

is the solar constant; substituting $\sigma = 5.67 \times 10^{-12}$ watt/cm^2 - °K^4, T_s = 6000°K (the sun's temperature), and ψ = 0.0093 the result is: C = 0.16 watt/cm^2; then for the mirror considered here, W = 7700 watts. However, due to loss of solar energy in the earth's atmosphere in the mirror and in the window of the vacuum chamber, amounting typically to 40% of the total radiant energy, the value of W in this case would be ~4600 watts. Also, if an object (e.g. the chamber housing the generator) is symmetrically located in the optical axis, a shadow is created in front of the mirror having an angle (θ_s) given by:

$$\tan \frac{\theta_s}{2} = \frac{R_s}{2f} \tag{A-7}$$

where R_s is the effective radius of the object; for R_s = 8" and f = 69, θ_s = 6° 40'. Due to the shadowing object a portion (W_s) of the solar energy is prevented from reaching the mirror. In the present case W_s ≈ 120 watts, computed from equation (A-5) after replacing θ_m by θ_s. This further reduces the solar energy into the cavity so that the net energy is approximately 4500 watts. The intensity at mirror's focal point is

$$I = \frac{W}{A_s} \tag{A-8}$$

where

$$A_s = \pi a^2 \tag{A-9}$$

Using W = 4500 watts and A_s = 0.885 $in.^2$ the intensity at the focal point becomes approximately 800 $watts/cm^2$.

For a given geometry of the cavity its optimum distance from the sun's image and consequently the optimum collection of the solar energy on the cavity surface depends on the intensity distribution on the sun's image (source). For a point source of uniform distribution and for a cavity with a reflecting rear surface the optimum cavity-source separation (H_1)(measured from the front surface of the cavity) is:

$$R = H_1 \tan \theta_m \qquad \text{(A-10)}$$

where R is the radius of the cylindrical cavity symmetrically located on the optical axis. For R = 0.61" and $\theta_m = 45°$, H_1 = 0.61". The curved surface of the cavity is formed by the rear surfaces of the six emitters of the converters. Part of the solar energy entering the cavity will impinge on these surfaces and to a great extent (~70%) will be absorbed; (these surfaces are made so as to have maximum absorptivity). The rest of the radiation entering the cavity will go through the rear opening of the cavity and stroke the reflector (reflectivity ~70%) designed to direct most of the reflected radiation back to the cavity surface.

2. CAVITY REFLECTOR

The design of the reflector is governed by the requirement that the reflected portion of the solar energy reaching the reflector is directed in its entirety to the cylindrical surface of the cavity formed by the back faces of the six emitters. This requirement can be readily satisfied by generating the reflector's surface through the revolution of a straight or curved line inclined at an appropriate angle with the optical axis, which

coincides with the cavity's geometrical axis. The resulting surface would assume the form of an inverted right cone with its apex on the optical axis. If the additional requirement is imposed that the reflected solar energy is uniformly distributed on the cylindrical cavity surface, the conical surface of the reflector would have to be generated by a curved line conforming to the profile of the intensity distribution of the solar energy from the source. Since the solid angle subtended at the source by the rear (circular) surface of the cavity above the reflector is not large, the solar flux intensity profile would not vary considerably along the segment intercepted by the reflector. Furthermore, if the reflector is to be made out of tungsten (electropolished), it will involve great difficulty and expense in accurately machining a cone having a surface generated by a curved (e.g. circular) line. Therefore, only a cone generated by a straight line will be considered here. However, such a cone, if made from a single surface, would have to be placed at an impractically long distance from the cavity in order to direct the whole reflected portion of the solar flux incident on the reflector back to the cylindrical wall of the cavity. To accomplish this and yet keep the reflector at a relatively short distance from the cavity a "double" cone, generated by two straight lines inclined at different angles to the optical axis would be suitable; such a cone is shown in the diagram of Figure A-2. The geometry of this cone (reflector) is discussed below.

The geometry of the reflector is conveniently determined by treating the transmission of light between the source, the cavity and the reflector as a two-dimensional problem of spatial symmetry. This is accomplished by assuming that the source (sun's image formed by the mirror) is a "point source" occupying the origin of a coordinate system with both the

cylindrical cavity and the conical reflector symmetrically located about the coordinate representing the optical axis. Referring to the diagram of Figure A-2, the solar energy incident on the reflector through the rear opening of the cavity is contained within a solid angle (ω) defined by the extreme light rays 1 and 3 making angles θ_1, and θ_s respectively with the vertical (optical axis); the solid angle is given by:

$$\omega = 2\pi (\cos \theta_s - \cos \theta_1), \tag{A-11}$$

where θ_s is the shadow angle, and

$$\tan \theta_1 = \frac{R}{H_2} , \tag{A-12}$$

where:

$$H_2 = H_1 + D \tag{A-13}$$

is the distance of the rear opening of the cavity from the source; D is the height of the cavity wall which is the same as the diameter of an emitter. For D = 0.658" and H_1 = 0.61", H_2 = 1.268" and hence, θ_1 = 25° 40' for R = 0.61". Since θ_s = 6° 40', ω = 0.578 steradians.

The total amount of solar enegy entering the cavity is contained within the solid angle (ω_c) defined by the angles θ_m and θ_s, i.e.

$$\omega_c = 2\pi(\cos \theta_s - \cos \theta_m) \tag{A-14}$$

For θ_s = 6° 40' and θ_m = 45°, ω_c = 1.80 sterad. The fraction of solar energy incident on the reflector is given by the radio ω/ω_c, i.e.

$$\frac{\omega}{\omega_c} = \frac{\cos \theta_s - \cos \theta_1}{\cos \theta_s - \cos \theta_m} \tag{A-15}$$

which, in this case, is 32%.

The reflector is formed by two inverted truncated cones (1 and 2) having their curved surfaces inclined at angles ϕ_1 and ϕ_2 respectively with the vertical. The value of each angle is such that all the reflected light from the corresponding cone (assuming specular reflection) is directed to the cavity wall, on which the light distribution is uniform throughout the total height (D) of the wall. The solar energy incident on cone 1 is contained within a solid angle (ω_1) defined by the rays 1 and 2 which make angles θ_1 and θ_2 respectively with the vertical; ω_1 is given by:

$$\omega_1 = 2\pi (\cos \theta_1 - \cos \theta_2) \qquad \text{(A-16)}$$

Upon reflection from the surface of cone 1, ray 1 impinges on the upper edge of the cavity wall (e.g. at H_1) while ray 2 strikes the lower edge of the wall, at a distance H_2 from the source. The solar energy incident on cone 2 is contained within the solid angle ω_2, defined by the rays 2 and 3, making angles θ_2 and θ_s respectively with the vertical; ω_2 is given by:

$$\omega_2 = 2\pi (\cos \theta_s - \cos \theta_2) \qquad \text{(A-17)}$$

Upon reflection from the surface of cone 2, rays 2 and 3 strike the upper (at H_1) and lower (at H_2) edges of the cavity wall respectively. The angles of inclination (ϕ_1 and ϕ_2) of the two truncated cones are given by:

$$\tan \phi_1 = \frac{x_1 - x_2}{y_2 - y_1} \qquad \text{(A-18)}$$

and

$$\tan \phi_2 = \frac{x_2 - x_3}{y_3 - y_2} \qquad \text{(A-19)}$$

where $y_2 - y_1$ is the height of cone 1 with radii of its bases x_1 and x_2, and $y_3 - y_2$ is the height of cone 2 with radii of its bases x_2 and x_3, as is evident from the diagram of Figure A-2. From the same diagram it can be seen that the ray angles θ_1, θ_2 and θ_s are related to the x-y coordinates of the two cones by the following equations:

$$\tan \theta_1 = \frac{x_1}{y_1} , \tag{A-20}$$

$$\tan \theta_2 = \frac{x_2}{y_2} , \tag{A-21}$$

and

$$\tan \theta_s = \frac{x_3}{y_3} . \tag{A-22}$$

For given cavity dimensions (R and D) and given light source extreme ray angles (θ_m and θ_s), a geometry for the conical reflector can be found to fulfill the requirement of directing all the reflected light to the cavity wall with uniform distribution along the wall height. This geometry, need satisfy the following relationships, evident from the diagram of Figure A-2:

$$\tan \gamma_1 = \frac{y_1 - H_1}{R + x_1} , \tag{A-23}$$

$$\tan \gamma_2 = \frac{y_2 - H_2}{R + x_2} , \tag{A-24}$$

$$\tan \gamma_2' = \frac{y_2 - H_1}{R + x_2} , \tag{A-25}$$

$$\tan \gamma_3 = \frac{y_3 - H_2}{R + x_3} \tag{A-26}$$

Any angle (γ) made by a reflected ray and the horizontal is related to

the angle (θ) made by the incident ray and the vertical and to the angle (ϕ) made by the reflecting surface and the vertical as follows:

$$\gamma = \frac{\pi}{2} - \alpha - \beta \tag{A-27}$$

where

$$\alpha = \frac{\pi}{2} - \phi \tag{A-28}$$

and also

$$\alpha = \theta + \beta \tag{A-29}$$

where β is the angle of incidence. Eliminating α and β from equation (A-27) it becomes:

$$\gamma = 2\phi + \theta - \frac{\pi}{2} \tag{A-30}$$

and consequently:

$$\tan \gamma = -\cot (2\phi + \theta) \tag{A-31}$$

where:

$$-\cot (2\phi + \theta) = \frac{\tan 2\phi \tan \theta - 1}{\tan 2\phi + \tan \theta} . \tag{A-32}$$

Also:

$$\tan \gamma = \frac{y - H}{R + x} \tag{A-33}$$

Combining equations (A-31), (A-32) and (A-33) one obtains:

$$\tan 2\phi = \frac{\left|\frac{y - H}{R + x}\right| \tan \theta + 1}{\tan \theta - \left|\frac{y - H}{R + x}\right|} \tag{A-34}$$

Introducing:

$$x = y \tan \theta \tag{A-35}$$

in equation (A-34) and rearranging it the result is:

$$\tan 2\varphi = \frac{2y - H + R \cot \theta}{y(\tan\theta - \cot\theta) + R + h \cot \theta} \tag{A-36}$$

Using equations (A-23), (A-24), (A-25) and (A-26), the above equation becomes:

$$\tan 2\phi_1 = \frac{2y_1 - H_1 + R \cot \theta_1}{y_1 (\tan\theta_1 - \cot \theta_1) R + H_1 \cot \theta_1} \tag{A-37}$$

$$\tan 2\phi_1 = \frac{2y_2 - H_2 + R \cot \theta_2}{y_2 (\tan \theta_2 - \cot \theta_2) + R + H_2 \cot \theta_2} \tag{A-38}$$

$$\tan 2\phi_2 = \frac{2y_2 - H_1 + R \cot \theta_2}{y_2 (\tan \theta_2 - \cot \theta_2) + R + H_1 \cot \theta_2} \tag{A-39}$$

$$\tan 2\phi_2 = \frac{2y_3 - H_2 + R \cot \theta_s}{y_3 (\tan \theta_s - \cot \theta_s) + R + H_2 \cot \theta_s} \tag{A-40}$$

Also, by introducing equations (A-20), (A-21) and (A-22) in equations (A-18) and (A-19) the two latter become

$$\tan \varphi_1 = \frac{y_1 \tan \theta_1 - y_2 \tan \theta_2}{y_2 - y_1} \tag{A-41}$$

$$\tan \varphi_2 = \frac{y_2 \tan \theta_2 - y_3 \tan \theta_s}{y_3 - y_2} \tag{A-42}$$

From the six equations (A-37) to (A-42) the six unknown parameters (φ_1, φ_2), θ_2, y_1, y_2, y_3) can be found. By combining equation A-37

and A-41 to eliminate y_1 and then combining the result with equation A-38 to eliminate ϕ_1 one obtains a solution for y_2 in terms of θ_2 and the known parameters θ_1, R, H_1 and H_2. Following the same procedure with equations (A-39), (A-40) and (A-42) (to eliminate y_3 and ϕ_2) one obtains another solution for y_2 in terms of θ_2 and the known parameters θ_s, R, H_1 and H_2; finally, by combining the two solutions, a result for θ_2 in terms of the known quantities θ_1, θ_s, R, H_1 and H_2 is obtained. This result is extremely complicated and will not be derived here. An alternate procedure, which does not involve the requirement of spreading the reflected light from cone 2 uniformly on the entire cavity wall, is to solve equation (A-37) to obtain ϕ_1, assuming y_1, constant; e.g. the value of y_1 may be dictated by the minimum cavity-reflector separation (h_o) that can be tolerated during assembly and operation. With ϕ_1 known, the combination of equations (A-38) and (A-41) results in the following equation:

$$y_2 = y_1 (\tan \theta_1 + \tan \phi_1) \left\{ \frac{[R + y_1 (\tan \theta_1 + \tan \phi_1)] \sin 2\phi_1 + H_2 \cos 2\phi_1}{R - H_2 \tan \phi_1 + 2y_1 (\tan \theta_1 + \tan \phi_1)} \right\} \quad \text{(A-43)}$$

where:

$$y_1 = h_o + h_2 \quad \text{(A-44)}$$

The angle θ_2 is subsequently derived from equation (A-21) after computing x_2 from equation (A-18).

If it is required that the second cone is so inclined as to direct ray 2 to the upper edge (at H_1) of the cavity wall, without regard of the direction of ray 3, the cone angle ϕ_2 can be found directly from equation (A-39). Alternately, if ray 2 is disregarded and it required only that the shadow-defining ray 3 strikes the lower edge (at H_2) of the cavity wall,

another value for ϕ_2, (ϕ_2') may be found from the following equation:

$$\sin\left[2\left(\phi_2' - \phi_1\right) - \left(\theta_2 - \theta_s\right)\right] = \sin\left(2\phi_1 + \theta_2 + \theta_s\right) - \sin 2\left(\phi_1 + \theta_2\right) \frac{\sin(\theta_1 + \theta_s)}{\sin(\theta_1 + \theta_2)} . \quad \text{(A-45)}$$

The above equation is readily derived from the geometrical relationships of the ray diagram shown in Figure A-2 and with the aid of equations (A-27), (A-28), and (A-29). By combining the two values of ϕ_2 computed from equations (A-3) and (A-45) an average value $\overline{\phi}_2$, $\left(\overline{\phi}_2 = \frac{\phi_2 + \phi_2}{2}\right)$ is obtained which fulfills the condition of directing the reflected light from cone 2 to the cavity wall evenly distributed about the middle of the wall but not necessarily covering the whole wall height (D). For the two values of ϕ_2 there are correspondingly two values of x_3, y_3, H_1 and H_2 computed from equations (A-22), (A-39), (A-40), (A-41) and (A-42) as follows:

For ϕ_2:

$$y_3 = \frac{y_2 \left(\tan\theta_2 + \tan\phi_2\right)}{\tan\theta_s + \tan\phi_2} \quad \text{(A-46)}$$

$$x_3 = y_3 \tan\theta_s , \quad \text{(A-47)}$$

$$H_2' = \frac{2y_3 + R\cot\theta_s \cdot \tan 2\phi_2 \left[R + y_2\left(\tan\theta_s - \cot\theta_s\right)\right]}{1 + \cot\theta_s \tan 2\phi_2} \quad \text{(A-48)}$$

For ϕ_2':

$$y_3' = \frac{y_2 \left(\tan\theta_2 + \tan\phi_2'\right)}{\tan\theta_s + \tan\phi_2'} \quad \text{(A-49)}$$

$$x_3' = y_3' \tan\theta_s \quad \text{(A-50)}$$

$$H_1' = \frac{2y_2 + R\cot\theta_2 - \tan 2\phi_2' \left[R + y_2\left(\tan\theta_2 - \cot\theta_2\right)\right]}{1 + \cot\theta_2 \tan 2\phi_2'} \quad \text{(A-51)}$$

The average values of the above parameters are then computed from the halfed sum of their corresponding dual values. In order to illustrate the application of the results of the above analysis the following example will be given. Let: $\theta_m = 45°$, $\theta_s = 6° 40'$, R = 0.61", D = 0.658" and $h_o = 0.10"$; then the unknown quantities assume the values presented in the table below.

REFLECTOR GEOMETRICAL PARAMETERS

Parameter:	H_1	H_2	θ_1	y_1	x_1	φ_1	y_2
Value:	0.610"	1.268"	25° 40′	1.368"	0.658"	47° 35′	1.610"
Equation #	A-10	A-13	A-12	A-44	A-20	A-37	A-42

Parameter:	x_2	θ_2	φ_2	φ_2'	$\bar{\varphi}_2$	y_3	x_3
Value:	0.393"	13° 40′	60° 40′	56° 35′	58° 40′	1.717"	0.201"
Equation #	A-18	A-21	A-39	A-45		A-46	A-47

Parameter:	H_2'	$\bar{H}_2$	y_3'	x_3'	$\bar{y}_3$	$\bar{x}_3$	H_1'
Value:	0.970"	1.120"	1.733"	0.203"	1.725"	0.202"	0.860"
Equation #	A-48		A-49	A-50			A-51

Parameter:	$\bar{H}_1$	β_1	β_2	$\bar{\beta}_{23}$	β_3
Value:	0.735"	16° 40′	28° 40′	17° 40′	24° 40′
Equation #		A-52	A-53	A-54	A-55

The angles (β) of incidence given in the above table are derived from the following equations:

$$\beta_1 = \frac{\pi}{2} - (\varphi_1 + \theta_1) \qquad \text{(A-52)}$$

$$\beta_2 = \frac{\pi}{2} - (\phi_1 + \theta_2) \tag{A-53}$$

$$\bar{\beta}_{23} = \frac{\pi}{2} - (\bar{\phi}_2 + \theta_2) \tag{A-54}$$

$$\beta_3 = \frac{\pi}{2} - (\bar{\phi}_2 + \theta_s) \tag{A-55}$$

The above example is illustrated in the diagram of Figure A-3. It can be readily deduced from the results presented above and from Figure A-3 that for a fixed reflector geometry (ϕ_1, ϕ_2) and cavity-reflector spacing (h_o) a limited vertical displacement (ΔH_1) of the source (along the optical axis) would not produce any significant changes of the concentration of the reflected solar energy on the cavity wall. For a given small source displacement the angles ϕ_1 and ϕ_2 may be chosen so as to permit all the reflected radiation to fall within the cavity wall height although at an uneven distribution. However, a small horizontal source displacement would cause some reflected radiant energy to escape the cavity wall. Figure A-4 presents a plot of ϕ_1 versus H_1 for different values of h_o and for R = 0.61", D = 0.658".

3. CAVITY-REFLECTOR RADIATION EXCHANGE

In order to compute the thermal radiation exchange between the reflector and the cavity, the radiation factor (F) between the cavity and the reflector must be known. Since the reflector is formed essentially by two surfaces, one conical and one flat, two view factors are involved in the exchange of radiation between cavity and reflector. For a net flow of thermal flux from surface 1 to surface 2, F is:

$$F_{12} = \frac{1}{\frac{1}{G_{12}} + (\frac{1}{\epsilon_1} - 1) + \frac{A_1}{A_2}(\frac{1}{\epsilon_2} - 1)} , \qquad (A-56)$$

where ϵ_1 and ϵ_2 are the total emissivities, of the two surfaces of corresponding areas A_1 and A_2. G_{12} is the geometrical view factor between the two surfaces, given by:

$$G_{12} = \frac{1}{A_1} \int_{A_1} \int_{A_2} \frac{\cos \delta_1 \cos \delta_2}{\pi s^2} \, dA_2 \, dA_1 , \qquad (A-57)$$

where δ_1 and δ_2 are the angles made by the normals to the two elements of area dA_1 and dA_2 and their distance s. For the case considered here and illustrated in the diagrams of Figures A-5 and A-6, A_1 represents the area of the cylindrical cavity, e.g.

$$A_1 = 2 \pi RD \qquad (A-58)$$

and A_2 is alternatively the area (A_3) of the flat circular portion of the reflector e.g.

$$A_3 = \pi x_3^2 , \qquad (A-59)$$

and that (A_2) of the conical section of the reflector, i.e.

$$A_2 = \pi \csc \phi \, (x_1^2 - x_3^2) \qquad (A-60)$$

The reflector conical section consists of two truncated cones 1 and 2 of apex half angles ϕ_1 and ϕ_2 respectively and of base radii x_1 and x_2 for cone 1 and x_2 and x_3 for cone 2. However, in order to simplify the present analysis only one cone of apex half angle $\phi = \tan^{-1}\left(\frac{x_1 - x_3}{y_3 - y_1}\right)$ and base radii x_1 and x_3 will be considered here.

The geometrical view factor (G_{13}) between the cylindrical cavity and the circular portion of the reflector is:

$$G_{13} = \frac{4R}{\pi A_1} \int_{h_2}^{h_1} \int_{o}^{\pi} \int_{o}^{x_3} \int_{o}^{\pi} \left[\frac{(R + x\cos\eta)\, hx}{(R^2 + h^2 + x^2 + 2Rx\cos\eta)^2} \right] d\eta\, dx\, d\eta\, dh \qquad \text{(A-61)}$$

The above equation is obtained from equation (A-57) after substituting A_2 by A_3 and δ_2 by δ_3 and introducing the following relationships, evident from Figure A-5:

$$dA_1 = R\, dh\, d\eta \qquad \text{(A-62)}$$

$$dA_3 = x\, dx\, d\eta \qquad \text{(A-63)}$$

$$\cos\delta_1 = \frac{R + x\cos\eta}{s} \qquad \text{(A-64)}$$

$$\cos\delta_3 = \frac{h}{s} \qquad \text{(A-65)}$$

$$s^2 = R^2 + h^2 + x^2 + 2Rx\cos\eta \qquad \text{(A-66)}$$

where $h = y_3 - H$. After integration, equation (A-61) becomes:

$$G_{13} = \frac{\pi}{2A_1}\left[h_2^2 - h_1^2 + \sqrt{h_1^4 + 2h_1^2(R^2 + x_3^2) + (R^2 - x_3^2)^2} - \sqrt{h_2^4 + 2h_2^2(R^2 + x_3^2) + (R^2 - x_3^2)^2} \right] \qquad \text{(A-67)}$$

where:

$$h_1 = y_3 - H_1 \tag{A-68}$$

and

$$h_2 = y_3 - H_2 \tag{A-69}$$

For R = 0.61" and D = 0.658", H_1 = 0.61", H_2 = 1.268", x_3 = 0.202" and y_3 = 1.725" as computed in Section 2; introducing these results in equation (67) one obtains: $G_{13} \approx 0.02$ for $A_1 = 2.52\ in^2$. Assuming that the cavity emissivity is $\epsilon_1 = 0.7$ and that of the reflector: $\epsilon_2 = 0.3$, equation (56), after replacing F_{12} by F_{13} and A_2 by A_3 results in $F_{13} = 0.0175$, for $G_{13} = 0.02$, $A_1 = 2.52\ in^2$ and $A_3 = 0.128\ in^2$; A_1 and A_3 were computed from equations (A-58) and (A-59). The net thermal flux (Q_{13}) from the cavity at temperature T_1 to the flat circular part of the reflector, at a temperature T_3, is:

$$Q_{13} = F_{13}\, A_1\ \sigma\ (T_1^4 - T_3^4) \tag{A-70}$$

which, for T_1 = 2000°K and T_3 = 1000°K is: Q_{13} = 24 watts.

The geometrical view factor (G_{12}) between the cylindrical cavity and the conical part of the reflector is:

$$G_{12} = \frac{4R\csc\phi}{\pi A_1} \int_{p_2}^{p_1} \int_{0}^{\pi} \int_{x_3}^{x_1} \int_{0}^{\pi} \left[\frac{x(R + x\cos\eta)(p\sin\phi + R\cos\phi\cos\eta)}{(R^2 + p^2 + x^2\csc^2\phi + 2Rx\cos\eta - 2px\cot\phi)^2} \right] d\eta'\, dx\, d\eta\, dp \tag{A-71}$$

The above equation is obtained from equation (A-57) after substituting:

$$dA_1 = R\, dp\, d\eta' \tag{A-72}$$

$$dA_2 = x\csc\phi\, dx\, d\eta \tag{A-73}$$

$$\cos \delta_1 = \frac{R + x \cos \eta}{s} \tag{A-74}$$

$$\cos \delta_2 = \frac{p \sin \phi + R \cos \phi \cos \eta}{s} \tag{A-75}$$

$$s^2 = R^2 + p^2 + x^2 \csc^2 \phi + 2 Rx \cos \eta - 2 px \cot \phi \tag{A-76}$$

and

$$p = y_3 + x_3 \cot \phi - H \tag{A-77}$$

Equations (A-72) to (A-77) above are readily established from the geometry of the diagram shown in Figure (A-6). After integrating twice between the limits 0 and π of the angles η, and η' equation(A-71) becomes

$$G_{12} = \frac{2\pi R}{A_1} \int_{p_3}^{p_1} \int_{x_3}^{x_1} \left[\frac{2R \{xpu_1 - 2x^2 u_1 \cot \phi + x^3 p(\csc^2 \phi - 2)\}}{\{u_1^2 - 4px u_1 \cot \phi + u_2 - u_3\}^{3/2}} + \frac{\cot \phi}{2R} \right] dx\, dp \tag{A-78}$$

where:

$$u_1 = p^2 + x^2 \tag{A-79}$$

$$u_2 = 2x^2 (2p^2 \cot^2 \phi + u_1 \csc^2 \phi - 2R^2) \tag{A-80}$$

$$u_3 = 4p x^3 \csc^2 \phi \cot \phi - x^4 \csc^4 \phi \tag{A-81}$$

$$p_1 = y_3 + x_3 \cot \phi - H_1 \tag{A-82}$$

and

$$p_3 = y_3 + x_3 \cot \phi - H_2 \tag{A-83}$$

Equation (A-78) was evaluated (in a computer program) for R = 0.677", D = 0.681", and for different values of x_1, x_3, p_1, p_3 and ϕ; the results of this computation along with the values of F_{12} computed for $\epsilon_1 = 0.7$ and $\epsilon_2 = 0.3$ are given below:

x_1	x_3	p_1	p_3	ϕ	A_1	G_{12}	A_2	F_{12}
0.792"	0.398"	1.567"	0.886	49°	2.89(in^2)	0.210	1.95(in^2)	0.115
0.905	0.445	1.767	1.086	52°	2.89	0.235	2.47	0.135
1.022	0.496	1.983	1.302	55°	2.89	0.262	3.06	0.155

For the case considered here, i.e., $R = 0.610"$, $D = 0.658"$, $x_1 = 658"$, $x_3 = 0.202"$, $\phi = 47° 35'$, $y_3 = 1.725"$, $H_1 = 0.735"$, $H_2 = 1.120"$, $p_1 = 1' 175"$, $p_2 = 0.790"$, $A_1 = 2.52\ in^2$ and $A_2 = 1.73\ in^2$ it is estimated that $G_{12} \approx 0.20$ and hence $F_{12} \approx 0.165$. The net flow of thermal energy (Q_{12}) from the cavity (at T_1) to the conical part of the reflector (at T_2) is:

$$Q_{12} = F_{12} A_1 \sigma (T_1^4 - T_2^4) \qquad \text{(A-84)}$$

Again, assuming $T_1 = 2000°K$ and $T_2 = 1000°K$, $Q_{12} = 226$ watts. Since the total thermal energy (Q) from the cavity into the reflector is:

$$Q = Q_{12} + Q_{13} , \qquad \text{(A-85)}$$

the above results indicate that $Q \approx 250$ watts.

4. SOLAR RADIATION

If all the solar energy (W) from the source (e.g., the image of the sun) enters the cavity part of it (W_1) will reach directly the cavity surface and the rest (W_2) will reach the reflector surface through the rear cavity opening. For a solar source of uniform intensity, W_2 is related to W by:

$$W_2 = \frac{\omega}{\omega_c} W \tag{A-86}$$

where $\frac{\omega}{\omega_c}$ (eq. 15) is the ratio of the solid angles subtended at the source by the front (ω_c) and rear (ω) openings of the cavity. Accounting for first reflections only from both the cavity and the reflector surfaces and assuming that both surfaces act as gray surfaces, and that all the initially reflected (specularly) radiation from the cavity strikes the reflector and vice-versa, then the net solar energy (W_c) absorbed by the cavity and that (W_R) absorbed by the reflector are:

$$W_c = \epsilon_1 (W_1 + W_{2r}) \tag{A-87}$$

and

$$W_R = \epsilon_2 (W_2 + W_{1r}), \tag{A-88}$$

where ϵ_1 and ϵ_2 are the total emissivities of the two surfaces.

Introducing:

$$W = W_1 + W_2 \tag{A-89}$$

$$W_{1r} = (1-\epsilon_1) W_1 \tag{A-90}$$

and

$$W_{2r} = (1-\epsilon_2) W_2 \tag{A-91}$$

equations (A-87) and (A-88) become:

$$\frac{W_c}{W} = \epsilon_1 \left(1-\epsilon_2 \frac{\omega}{\omega_c}\right) \tag{A-92}$$

and

$$\frac{W_R}{W} = \epsilon_2\left[1 - \epsilon_1 \left(1-\frac{\omega}{\omega_c}\right)\right]. \tag{A-93}$$

The fraction (f_o) of solar energy:

$$f_o = 1-\left(\frac{W_c}{W} + \frac{W_R}{W}\right) = 1 -(\epsilon_1 + \epsilon_2 - \epsilon_1\epsilon_2) \tag{A-94}$$

is assumed to be lost by reflection through the front opening of the cavity. For the case considered here ($\frac{\omega}{\omega_c} = 0.32$, $\epsilon_1 = 0.7$, $\epsilon_2 = 0.3$), $\frac{W_c}{W} = 0.633$, $\frac{W_R}{W} = 0.157$, and $f_o = 0.210$; hence, for W = 4600 watts (eq. 6), $W_c \approx 2,910$ watts, (485 watts on each of the six emitters), and $W_R = 720$ watts. The input power densities to the cylindrical cavity of area $A_1 = 2.52$ in^2 and to the conical part of the reflector of area $A_2 = 1.73$ in^2, are:
$\frac{P_c}{A_1} \approx 165 \frac{\text{watts}}{\text{cm}^2}$ and $\frac{P}{A_2} \approx 85 \frac{\text{watt}}{\text{cm}^2}$ respectively; P_c and P are the total input powers to the cavity and the reflector respectively, i.e.:

$$P_c = W_c - Q \tag{A-95}$$

$$P = W_R + Q \tag{A-96}$$

In the present case $P_c = 2660$ watts and $P \approx 970$ watts.

The reflector temperature (T_2) is controlled by the rate of radiation and conduction heat losses from the rear part (radiator) of the reflector.

The front part of the reflector, facing the cavity is made out of electro-polished tungsten to assure a high reflectivity (e.g. $\varepsilon_2 \approx 0.3$). The rear part is made out of molybdenum with Cr_2O_3 surface to assure a high radiation rate; the two parts are brazed together and fastened by screws through to the molybdenum frame holding the converters. Although a small amount of heat may be transferred from the back piece to the frame, most of the heat absorbed by the reflector will be dissipated by radiation to the surroundings from the radiator.

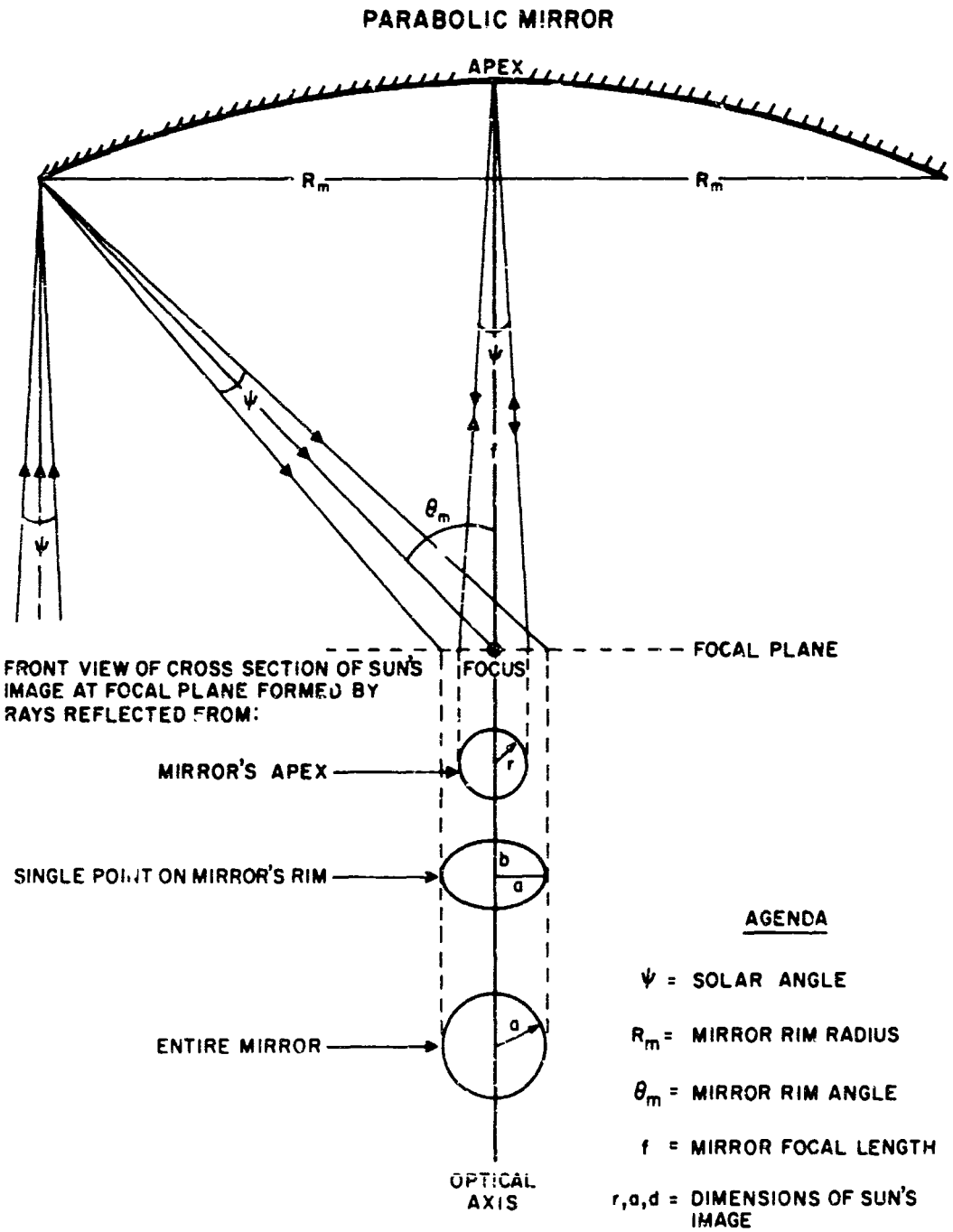

Figure A-1. Sun's Image from Parabolic Mirror Used in the JG-4 Generator.

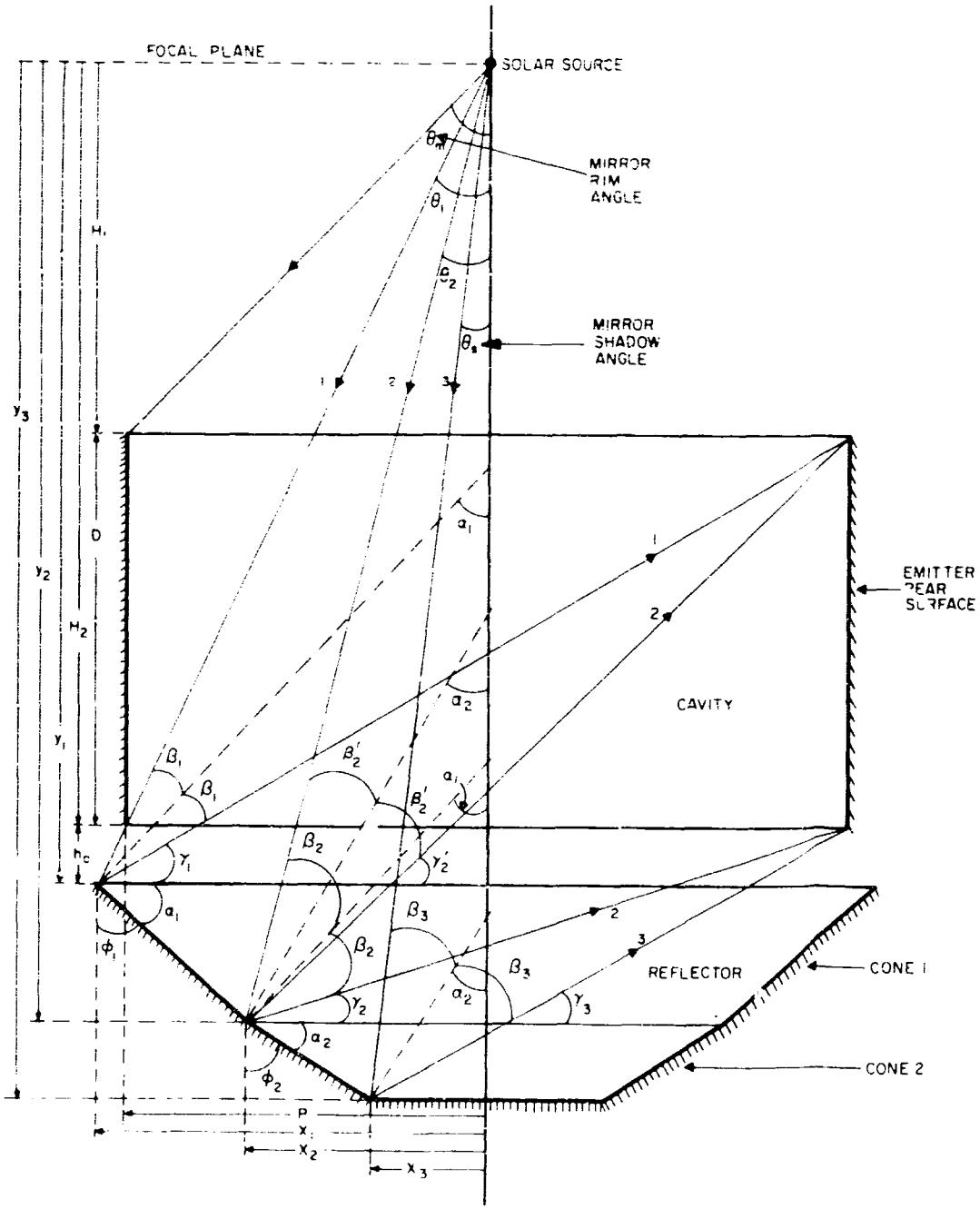

Figure A-2. Reflection of Solar Flux from Conical Reflector Placed at Bottom of Cavity in the JG-4 Generator.

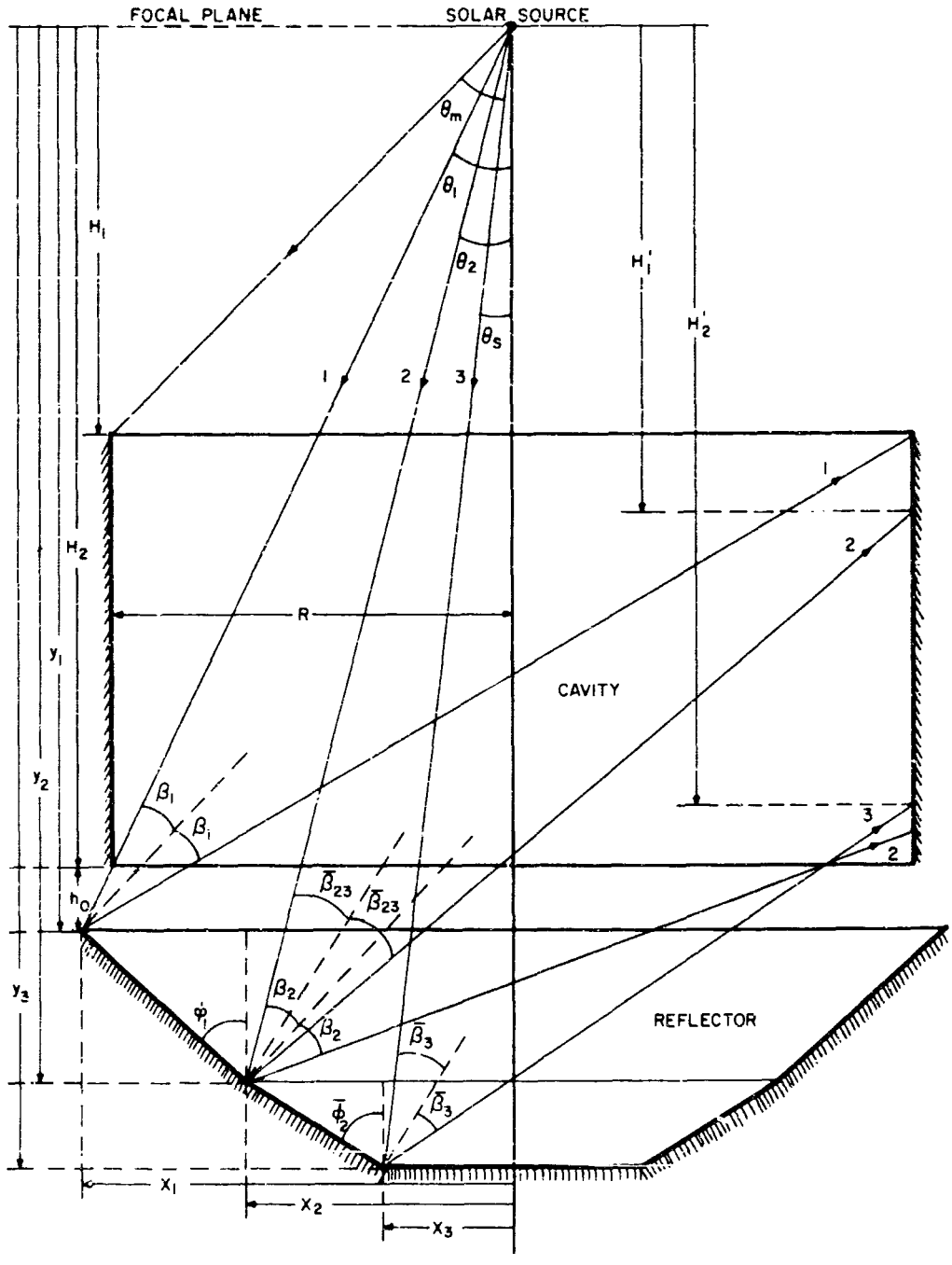

Figure A-3. Computed Paths of Reflected Rays Defining Solar Flux Incident on Reflector (Cavity-Reflector Geometry in 5:1 Scale).

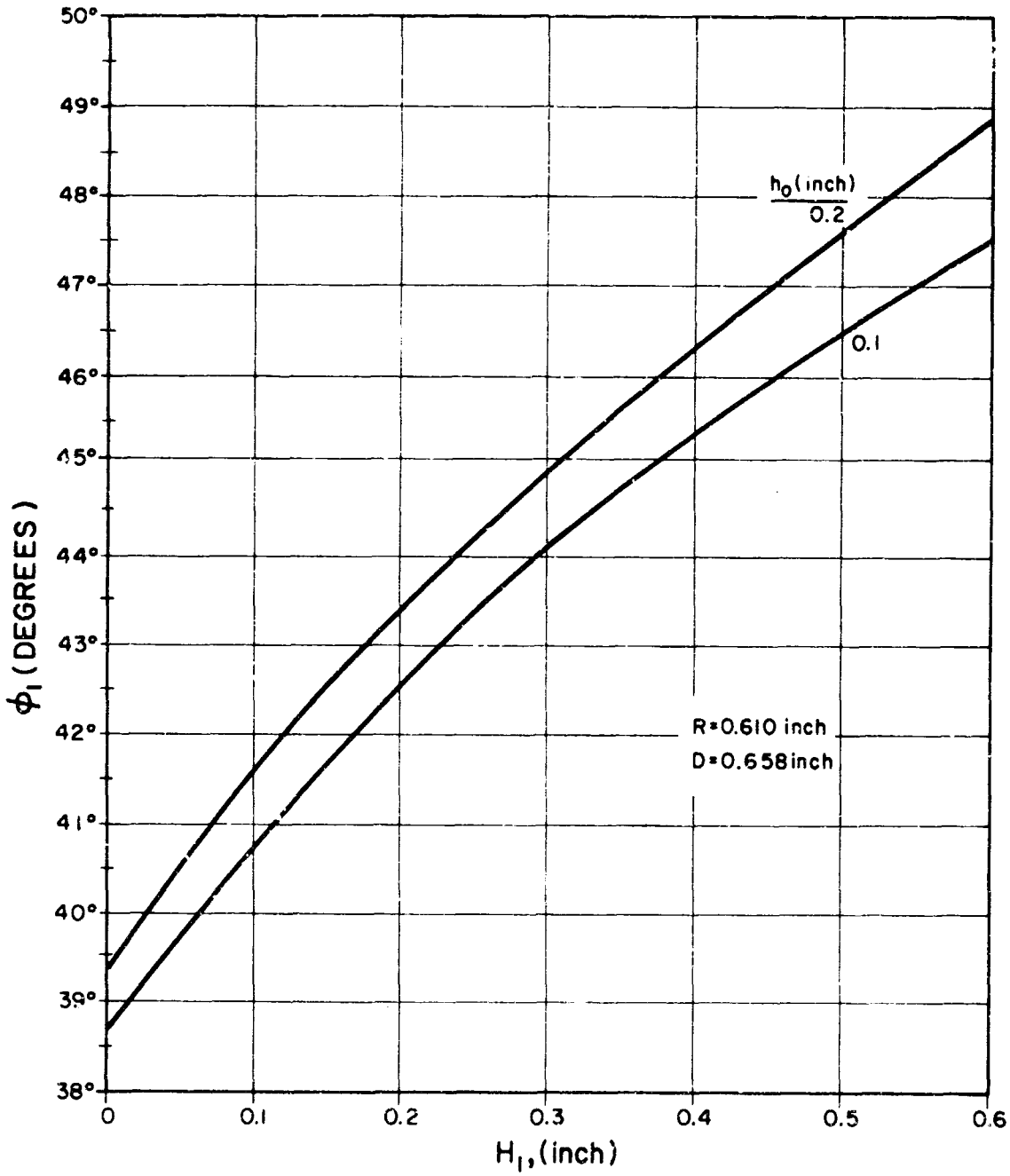

Figure A-4. Variation of Angle of Inclination (φ_1) of Reflector Cone 1 with Distance (H_1) of Solar Source from Cavity.

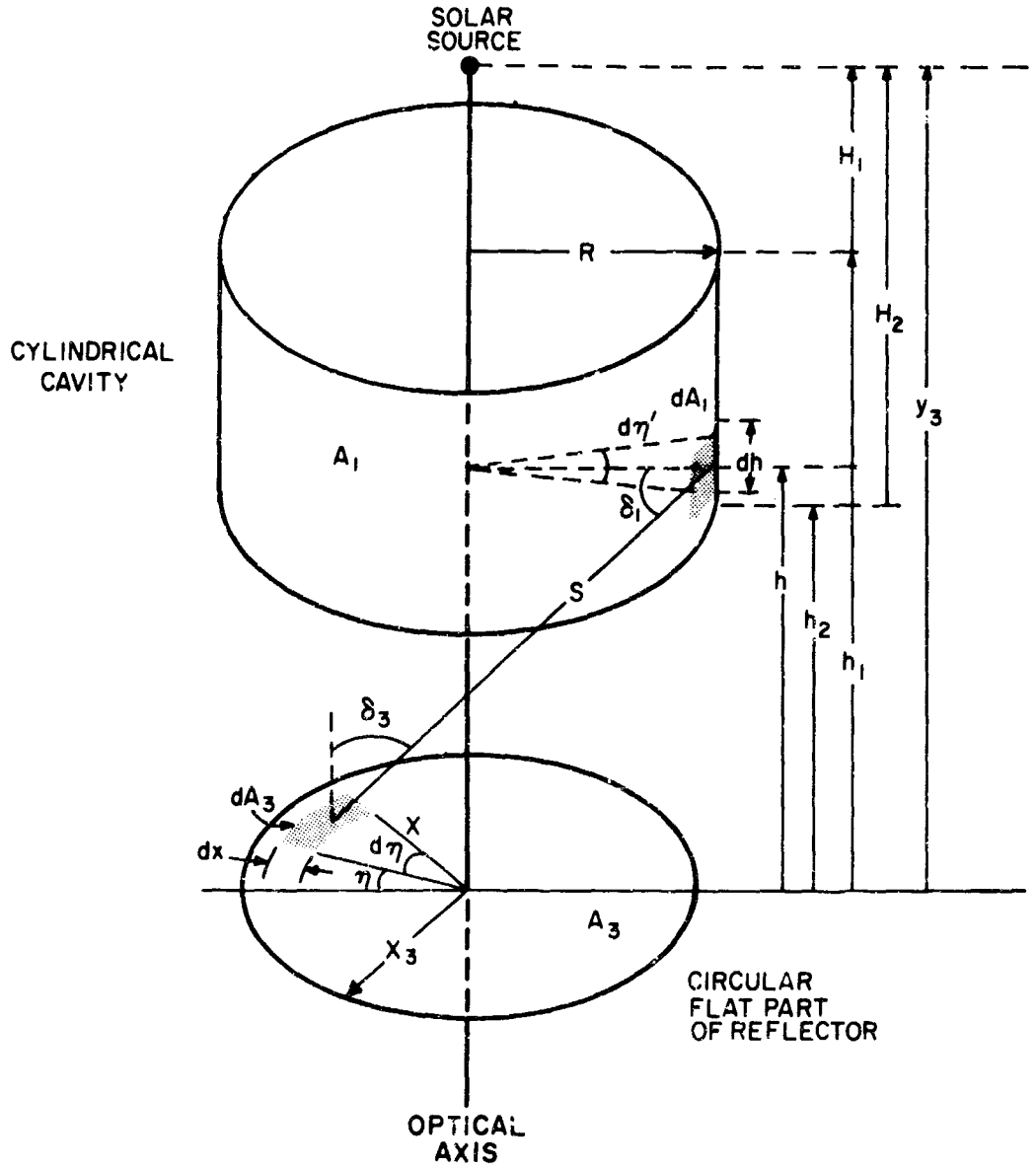

Figure A-5. Diagram for Deriving Geometrical View Factor Between Cavity and Flat Part of Reflector.

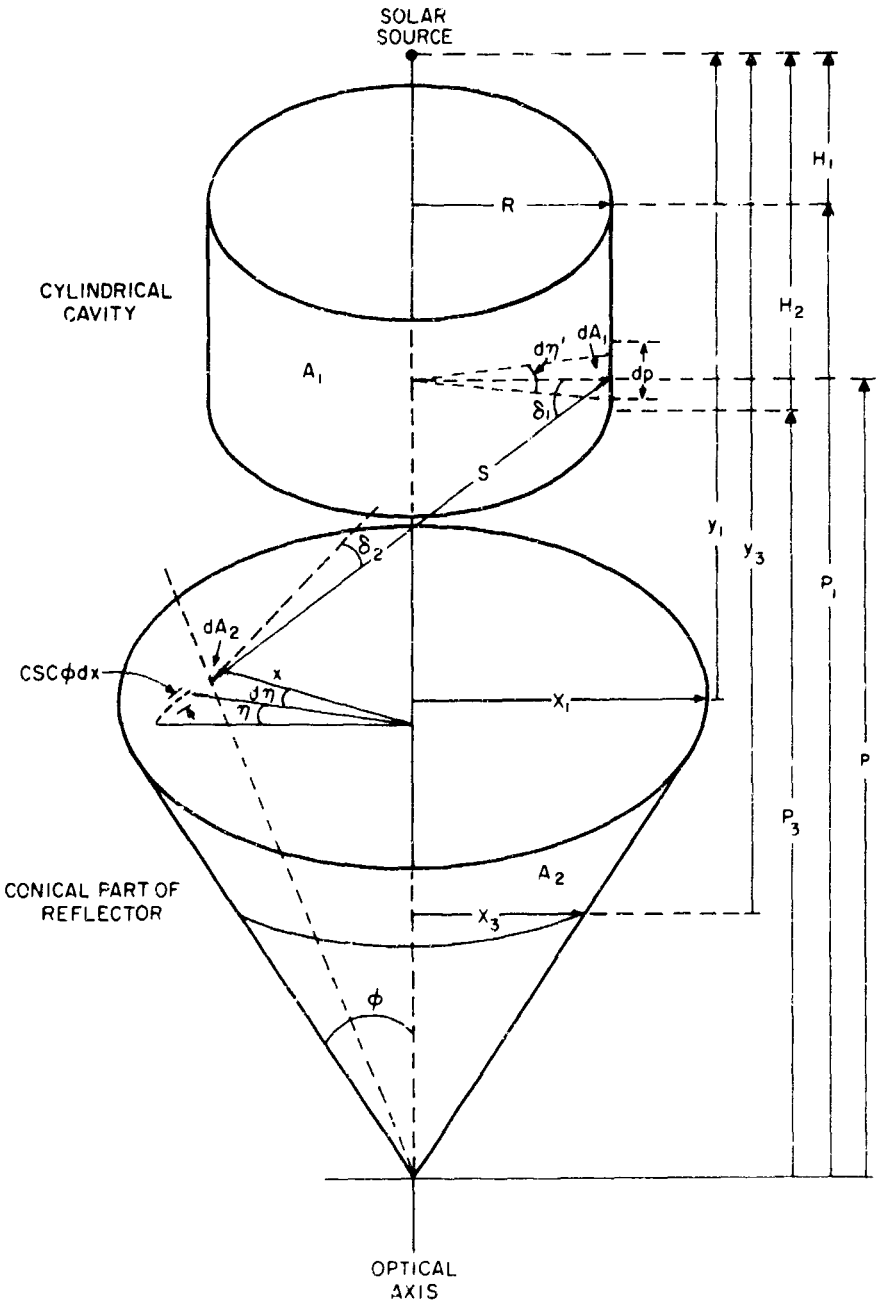

Figure A-6. Diagram for Deriving Geometrical View Factor Between Cavity and Conical Part of Reflector.

APPENDIX B

DETAILED ANALYSIS OF MODIFIED CAVITY BACK-PIECE FOR THE JG-4

RADIANT ENERGY DISTRIBUTION IN THE CAVITY OF THE SIX-CONVERTER SOLAR THERMIONIC GENERATOR (JG-4)

Recent theoretical and experimental data supplied by JPL indicated that the intensity distribution of the solar energy at the region of the solar image created by the parabolic mirror in front of the cavity is different from the distribution previously assumed in computing the radiant flux transfer in the various parts of the cavity. Some of the JPL data are reproduced in Figure B-1 and Table B-I; Figure B-1 shows plots of the solar intensity ratio (I/I_m) versus the relative radius (r/r_i) of the solar image for different distances (d) from the focal plane. I_m is the maximum intensity of the solar flux, which is approximately 1750 watts/cm^2; r_i = 1.346 cm is the theoretical radius of the solar image. The plots were constructed for distances above the focal plane (nearer the sun), but practically identical plots can be obtained for corresponding distances below the focal plane. Figure B-2, constructed from the data of Figure B-1, shows the spatial distribution of equal-intensity profiles about the solar image.

The data of Table B-I show the solar energy distribution in the cavity for four of the most promising mirror-cavity arrangements characterized by focal plane-aperture separations ranging from 0 to 1.5 cm and all including the vacuum glass envelope of the generator. For comparison purposes, a fifth arrangement which does not include the glass envelope and which produces the maximum solar flux (~5000 watts) input to the cavity is also presented in Table B-I. Among the first four arrangements Nos. 2 and 3 seem to indicate the optimum focal plane-aperture separation (0.5 - 1.0 cm) that results in high initial flux input to the emitters (290 - 310 watts each), without excessive loss of flux outside the cavity (70 - 570 watts), and without too high a flux input to the cavity back-piece (2050 - 2720 watts). Since photographs of the solar image showed a second

maximum for the solar energy in front of the focal plane (nearer the sun or the cavity), it may be concluded that the 1-cm focal plane-aperture separation (arrangement #3) would produce the near-optimum solar flux distribution in the cavity.

In view of the above discussion and for the purpose of estimating the amount of radiant energy transferred to the various parts of the cavity when arrangement #3 is employed, it will be assumed that a solar energy of about 4500 watts penetrates the glass envelope and that a portion of it consisting of 4300 watts enters the cavity with 1800 watts initially incident on the emitters and 2500 watts incident on the back-piece. For comparison purposes arrangement #5 is also considered; in this arrangement, where the focal plane coincides with the cavity aperture and the glass envelope is not present, the whole solar flux (5,000 watts) reflected by the mirror enters the cavity with 1500 watts initially incident on the emitters and 3500 watts incident on the back-piece. For these two arrangements (#3 and #5) the radiant energy distribution in the cavity is presented analytically in Tables B-II and B-III for different back-piece materials selected for their promising thermal and optical properties given in Table B-IV. For arrangement #3 three materials, e.g. W, Ta, and Ni, are considered; in this case both the front and rear parts of the back-piece are made out of the same material. In arrangement #5 these parts are made both out of Al or from combinations of other materials such as: W-Mo, W-Cu, and Au-Cu.

Tables B-II and B-III were constructed using the emissivity and reflectivity data of Table B-IV and utilizing the results of the following analysis for the radiant flux distribution in the cavity. This analysis considers only first reflections (specular) of the solar radiation in the cavity and assumes that all the radiation reflected by the back-piece reaches first the cylindrical wall (continuous) formed by the rear surfaces of the six emitters in the cavity; part of this radiation is reflected to the front-piece and escapes

through the aperture. Correspondingly all the radiation initially reflected by the emitters reaches first the back-piece, from which the portion reflected is directed to the front-piece and escapes through the aperture. The solar energy incident on the front-piece is partly absorbed and partly reflected back to the mirror. Under these assumptions the amounts of solar energy absorbed by the front-piece (W_o), by the emitters (W_1), and by the back-piece (W_2) are:

$$W_o = (1 - r_o) S_o, \tag{B-1}$$

$$W_1 = (1 - r_1)(S_1 + r_2 S_2), \tag{B-2}$$

and

$$W_2 = (1 - r_2)(S_2 + r_1 S_1), \tag{B-3}$$

where S_o, S_1, and S_2 are the amounts of solar energy initially incident on the front-piece, the emitters, and the back-piece, having reflectivities r_o, r_1, and r_2, respectively. The amount of solar energy (U) escaping through the aperture is:

$$U = r_1 r_2 (S_1 + S_2) \tag{B-4}$$

The total input energy to the emitters (P_1) and to the back-piece (P_2) is computed by accounting for the net amount of the thermal energy (Q) transferred from the emitters, maintained at a temperature T_1, to the back-piece, maintained at a temperature T_2 ($T_2 < T_1$), while neglecting any thermal energy transfer between emitters and front-piece, e.g.,

$$P_1 = W_1 - Q, \tag{B-5}$$

and

$$P_2 = W_2 + Q. \tag{B-6}$$

Q is given by:

$$Q = F A_1 \sigma (T_1^4 - T_2^4) \tag{B-7}$$

where:

$$F = \frac{1}{\frac{1}{G} + \left(\frac{1}{\epsilon} - 1\right) + \frac{A_1}{A_2}\left(\frac{1}{\epsilon}_2 - 1\right)} \qquad \text{(B-8)}$$

is the radiation factor between the emitters and the front part of the back-piece, having areas and total emissivities A_1, ϵ_1, and A_2, ϵ_2, respectively; G is the geometrical view factor between A_1 and A_2. For the case considered here $A_1 \approx 16.3$ cm^2, $A_2 \approx 12$ cm^2, and $G \approx 0.2$. The area (A_2) of the rear part of the back-piece from where the absorbed power is dissipated by radiation is determined from:

$$A_3 = \frac{P_3}{\sigma \epsilon_3 T_3^4}, \qquad \text{(B-9)}$$

where T_3 and ϵ_3 are the average temperature and total emissivity of the rear part, assumed much hotter than its surroundings, and P_3 is the radiated power; neglecting any conduction losses in the back-piece, $P_3 = P_2$.

The front-piece, where the aperture is located, has a truncated conical surface facing the mirror and inclined at an angle of 52° with the cavity axis; the area (A_o) of this surface is about 120 cm^2. Assuming that the solar radiation falling outside the cavity is evenly distributed on the whole conical surface, and that no radiation exchange takes place between the front-piece and the six converters, then the average temperature (T_o) of this piece may be computed from:

$$T_o^4 \approx \frac{W_o}{\sigma \epsilon_o A_o} \qquad \text{(B-10)}$$

where ϵ_o is the total emissivity of the conical surface, and W_o is given by equation 1. The aperture of 2.54-cm diameter is located at about 0.28 cm away from the top of the cylindrical cavity which is 1.66 cm high and has a 3.1-cm diameter. The bottom of the cavity is about 0.30 cm

away from the opening of the conical front part of the back-piece. Some of the above dimensions are slightly different from those used by JPL in deriving the data of Table B-I, but these differences are too small to introduce any significant effect on the distribution of the solar energy in the cavity.

The design of the conical front part of the back-piece is based on the assumption that the solar energy entering the cavity emanates from a point-source at a distance of 1.27 cm from the aperture. For an extended source, e.g., a solar image of radius 1.346 cm placed at a different distance (e.g., 1 cm) from the aperture a new design may be required for satisfying the condition that all the solar flux reflected by the back-piece reaches first the emitters in the cavity. Since a detailed study (in a computer program) is currently conducted by JPL to determine the optimum configuration of the front part of the back-piece for different mirror-cavity arrangements no attempt will be made to alter the present design which may be found nevertheless to be adequate for causing the major portion of the back-piece-reflected solar energy to impinge on the emitters in the cavity.

The design of the rear part of the back-piece is changed to accommodate the most unfavorable mirror-cavity arrangement (#5) where a solar flux of 3500 watts impinges on this piece. For this case a large surface is required for dissipating by radiation the absorbed energy and preventing the temperature of the back-piece to assume undesirable values (e.g., above 1200°K). In view of the desired radiant energy distribution in the cavity and because of space and weight limitations of the present overall generator design and also because of restrictions on converter contamination from evaporating materials the data of Table B-III indicate that the most promising choice of materials for the back-piece is W for the front and Mo for the rear part. W and Mo can be readily joined (brazed) by high-melting point (e.g., above 1500°K) alloys such as 0.65 Pd-0.35 Co, or 0.465 Mo-0.535 Ni. For the W-Mo combination of the back-piece the radiating area (A_3) of the rear part is about 430 cm^2,

allowing the Mo piece to be maintained at an average temperature of 1000°K while the W front piece is at about 1200°K, with both materials having very low evaporation rates at these temperatures. Although W is a better heat conductor than Mo, it is about twice as heavy and more expensive in original cost and fabrication than Mo. Therefore, W is used only in the front (small) part of the back-piece where its higher reflectivity makes it more desirable than Mo.

The emissivity data of Table IV were taken from Figure 3 where the total emissivity of different materials is plotted versus temperature; the plots of Figure 3 were constructed from data given by various sources indicated in the same figure. The reflectivity data of Table IV were estimated from the plots of spectral reflectivity of different (polished) materials shown in Figure 4, which also indicates the sources of the original data. The reflectivity of polished tungsten was assumed equal to 0.55, slightly lower than that derived from available data as follows: The spectral reflectivity (r_λ) at room temperature and the spectral emissivity (ϵ_λ) at 1600°K were first plotted versus wavelength (λ) as shown in Figure 5 where the sources of the original data are also indicated. Data for ϵ_λ at 2200°K result in a practically identical plot as that for ϵ_λ at 1600°K indicating that ϵ_λ is essentially independent of the material (tungsten) temperature (T_W); this fact is evident from the original data and also from Figure 6. Assuming that the spectral absorptivity (α_λ) and reflectivtivity (r_λ) are independent of temperature then the total absorptivity (α) and reflectivity (r) may be computed from:

$$\epsilon = \int_0^\infty \epsilon_\lambda I_\lambda (T)\, d\lambda \Big/ \int_0^\infty I_\lambda (T)\, d\lambda, \qquad (B\text{-}11)$$

and

$$r = \int_0^\infty r_\lambda I_\lambda (T)\, d\lambda \Big/ \int_0^\infty I_\lambda (T)\, d\lambda, \qquad (B\text{-}12)$$

where I_λ is the relative spectral intensity of the solar radiation at temperature T. Using the data for I_λ (T) on the earth's surface supplied by JPL and plotted in Figure 6 for the data for r_λ and ϵ_λ presented in Figure B-5, the curves for $I_\lambda r_\lambda$ and $I_\lambda \epsilon_\lambda$ were obtained and plotted in Figure B-6. By measuring the areas under these curves and computing their ratio, according to Equations B-11 and B-12 (within given limits for λ), it was found that $\alpha \approx 0.394$ ($T_W = 1600°K$), $\alpha = 0.388$ ($T_W = 2200°K$), and $r = 0.598$ ($T_W = 300°K$); these results are in good agreement with the theoretical prediction: $\alpha + r = 1$. The emissivity and reflectivity of the grooved Re emitter surfaces and the emissivity of the grooved and Cr_2O_3-coated surface of the rear part of the back-piece were assumed equal to 0.70, 0.25 and 0.75 respectively, according to experimental data obtained in the past.

The temperature (T_3) for the different materials suggested for the rear part of the back-piece was estimated from the maximum tolerable temperature (T_2) of the front part material and the thermal conductivity and overall geometry of the back-piece. The data for the thermal conductivity and evaporation rate at the temperatures of interest for the various materials presented in Table B-IV were obtained from the following sources: W. H. Kohl, "Materials and Techniques for Electron Tubes" (1960); S. Dushman, "Vacuum Technique" (1958); Thermophysical Properties Research Center, Purdue University, Data Book, Vol. I (1966).

TABLE B-I

SOLAR FLUX DISTRIBUTION IN CAVITY

(All amounts of flux are approximate. Energy at focal plane is ~5010 watts)

Mirror-Cavity Arrangement #	Focal Plane-Aperature Separation (cm)	Flux Outside Cavity (watt)	Cavity Flux Distribution (watt)			
			Total	Six Emitters	One Emitter	Back-Piece
1	0	90	4420	1080	180	3340
2	0.5	70	4440	1720	290	2720
3	1.0	570	3940	1890	310	2050
4	1.5	1290	3220	1730	290	1490
5	0 (No Glass)	10	5000	1500	250	3500

TABLE B-II

CAVITY RADIATION DATA

(Arrangement #3; Total Energy into Cavity = 4500 watts)

Back-Piece Material	Radiant Energy Distribution (watt)							
	FRONT-PIECE (W-Polished; T_o=1000°K)			EMITTERS (Re-grooved; T_1 = 2000°K)				
	Incident S_o	Absorbed W_o	Escaped through Aperture U	Incident S_1	Absorbed W_1	Radiated Q	Total Absorbed 6 Emitters P_1	Total Absorbed 1 Emitter $P_1/6$
W	200	90	590	1800	2380	-90	2290	380
Ta	200	90	530	1800	2290	-90	2200	370
Ni	200	90	700	1800	2570	-90	2480	415

	BACK-PIECE							
	Front Part (Polished)					Rear Part (Grooved and Cr_2O_3-Coated)		Unused Solar Energy
	Temp (°K) T_2	Incident S_2	Absorbed W_2	Radiated Q	Total Absorbed P_2	Temp (°K) T_3	Radiating Area (cm^2) A_3	$S_o + U + P_2$
W	1200	2500	1300	90	1420	1000	335	2210
Ta	1200	2500	1480	90	1570	900	565	2300
Ni	900	2500	1030	90	1120	700	1100	1850

TABLE B-III

CAVITY RADIATION DATA

(Arrangement #5; Total Energy into cavity = 5000 watts)

Radiant Energy Distribution (watt)

Back-Piece Materials Combination	EMITTERS (Re-grooved; T_1 = 2000°K)						
				Total Absorbed		Escaped through	Total
	Incident S_1	Absorbed W_1	Radiated Q	Six Emitters P_1	One Emitter $P_1/6$	Aperture U	Unused $U+P_2$
W-Cu	1500	2570	-80	2490	415	690	2510
W-Mo	1500	2570	-80	2490	415	690	2510
Au-Cu	1500	2960	-30	2930	480	880	2070
Al-Al	1500	2960	-50	3170	530	1000	1830

BACK-PIECE

Front Part (Polished)						Rear Part (Grooved and Cr_2O_3-Coated)		
Material	Temp (°K) T_2	Incident S_2	Absorbed W_2	Radiated Q	Total Absorbed P_2	Material	Temp(°K) T_3	Radiating Area (cm^2) A_3
W	1000	3500	1740	80	1820	Cu	900	650
W	1200	3500	1740	80	1820	Mo	1000	430
Au	900	3500	1160	30	1190	Cu	850	540
Al	800	3500	780	50	830	Al	750	620

TABLE B-IV

PROPERTIES OF CAVITY MATERIALS

Material	Temp. (^{o}K)	Total Reflectivity	Total Emissivity	Evaporation Rate (gm/cm^{2}-sec)	Thermal Conductivity (watt/cm-K^{o})
FRONT-PIECE (Polished)					
	T_o	r_o	ϵ_o		
W	1000	0.55	0.11	5×10^{-34}	1.20
EMITTERS (grooved)					
	T_1	r_1	ϵ_1		
Re	2000	0.25	0.70	8×10^{-14}	0.47
BACK-PIECE					
Front Part (Polished)					
	T_2	r_2	ϵ_2		
Al	800	0.80	0.06	3×10^{-13}	2.25
Au	900	0.70	0.03	3×10^{-14}	2.80
Ni	900	0.65	0.12	1×10^{-14}	0.70
Ta	1200	0.50	0.14	1×10^{-25}	0.60
W	1000	0.55	0.11		1.20
W	1200	0.55	0.13	8×10^{-28}	1.15
Rear Part (Grooved and Cr_2O_3 - Coated)					
	T_3		ϵ_3		
Al	750		0.75		2.30
Cu	850		0.75		3.65
Ni	700		0.75		0.65
Ta	900		0.75		0.60
Cu	900		0.75	4×10^{-13}	3.60
Mo	1000		0.75		1.10

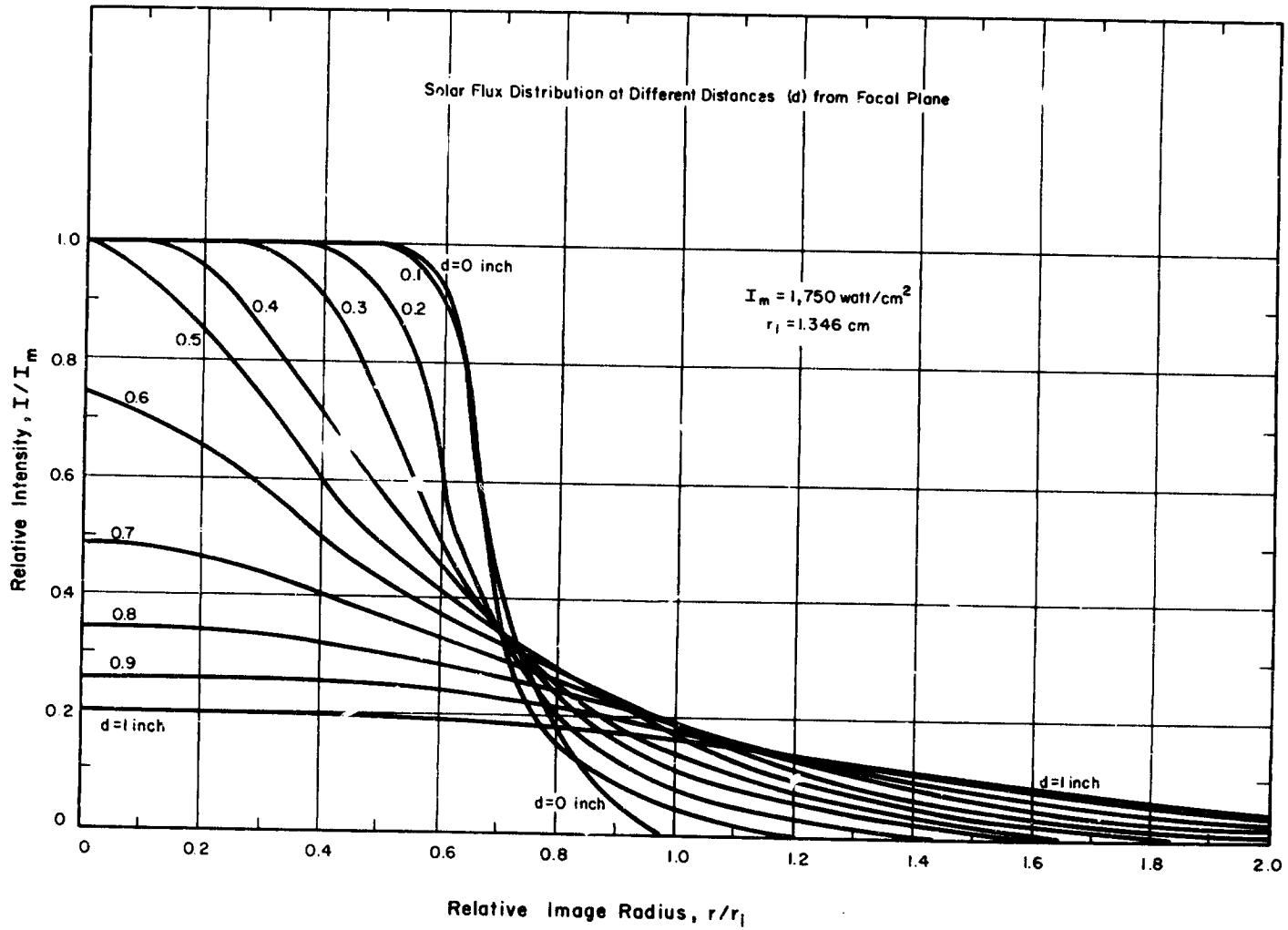

Figure B-1. Solar Flux Distribution at Different Distances from Focal Plane.

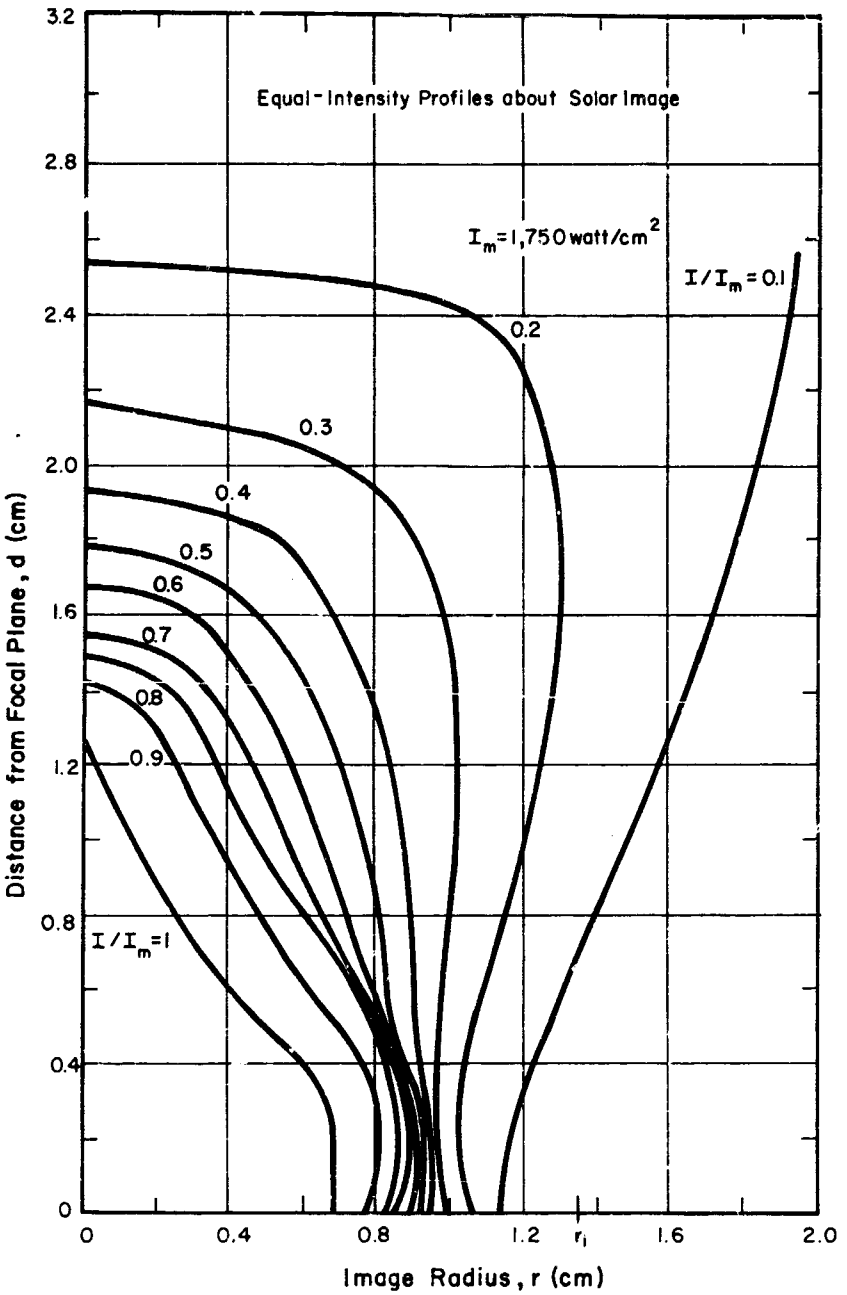

Figure B-2. Equal-Intensity Profiles about Solar Image.

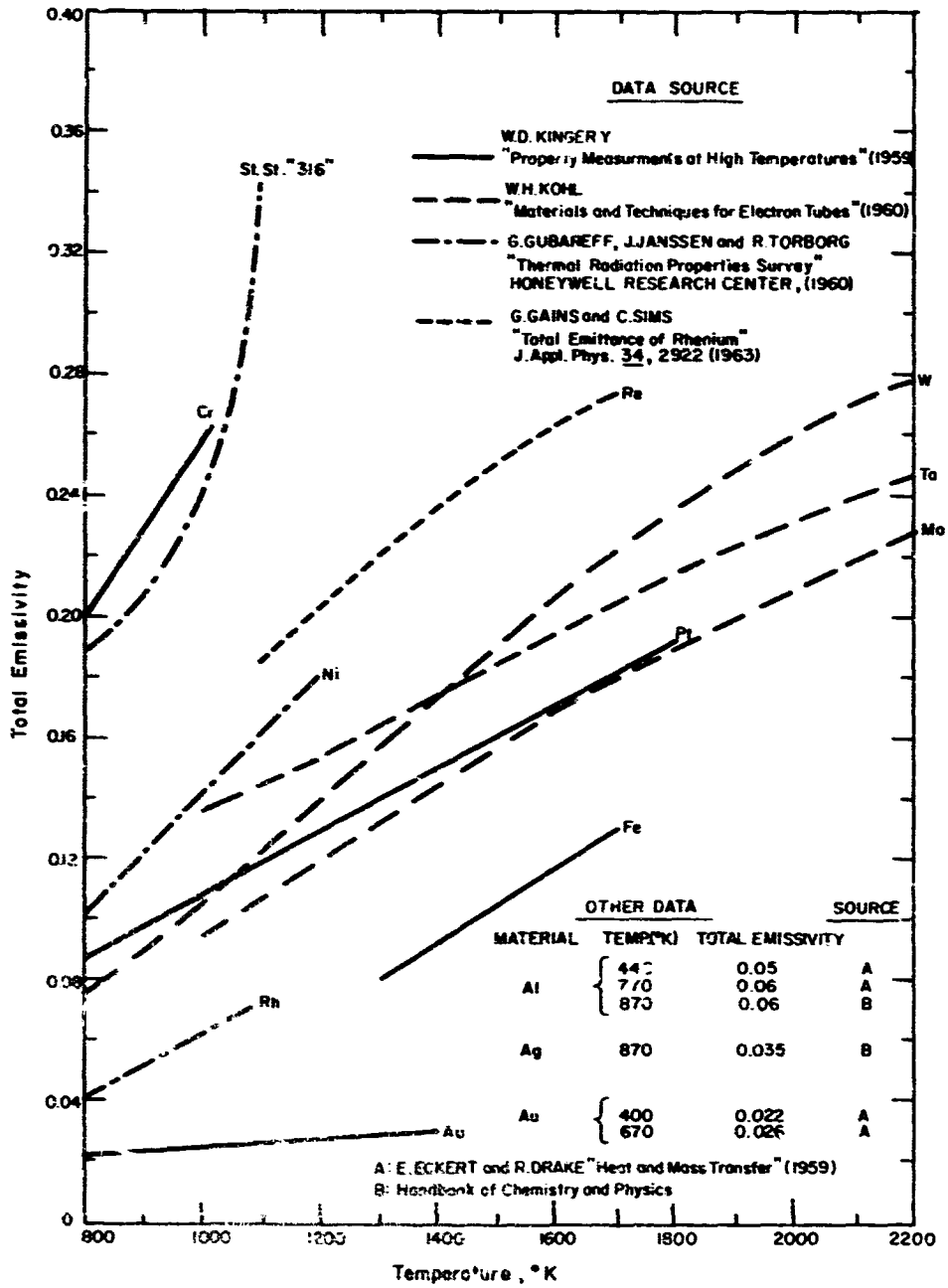

Figure B-3. Total Emissivity of Different Materials.

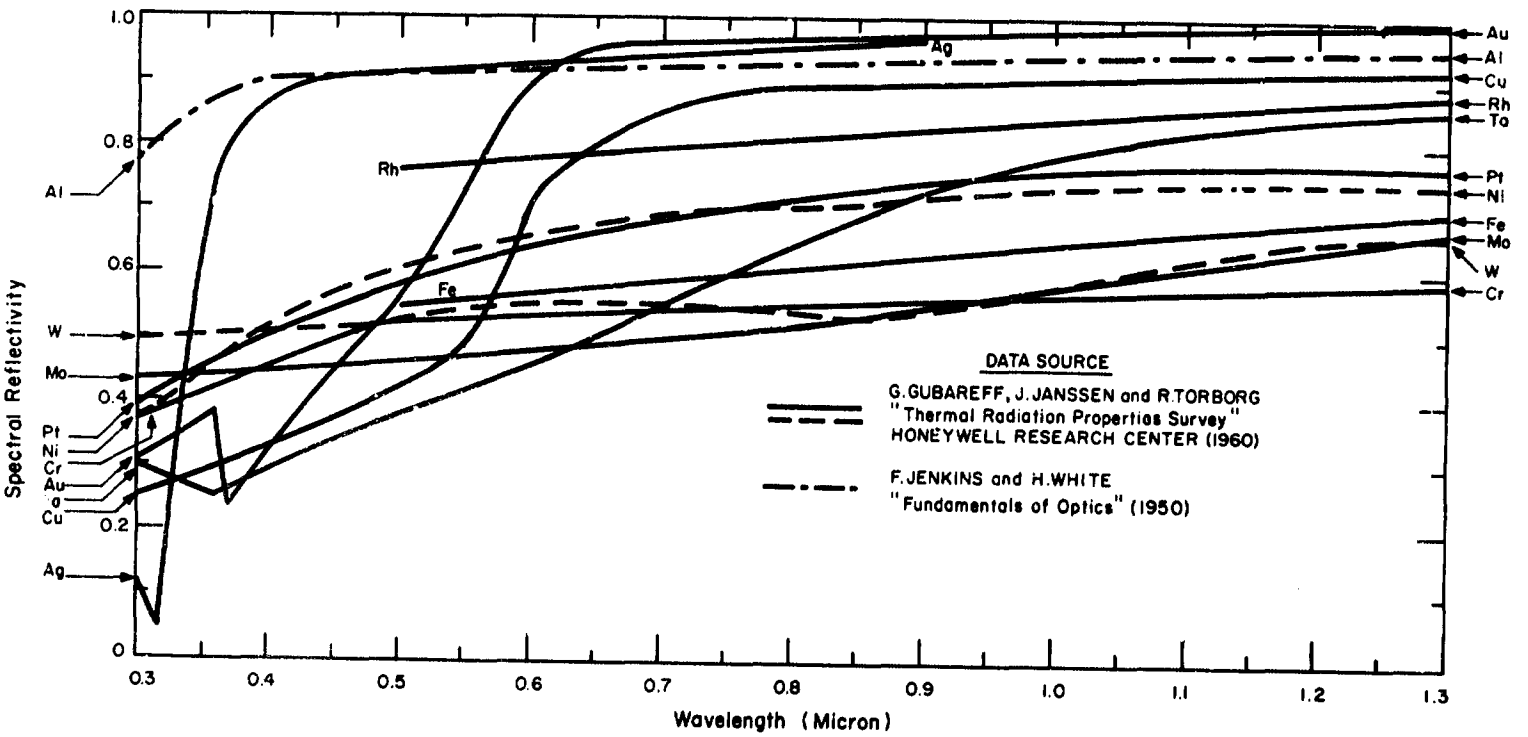

Figure B-4. Spectral Reflectivity of Different Materials.

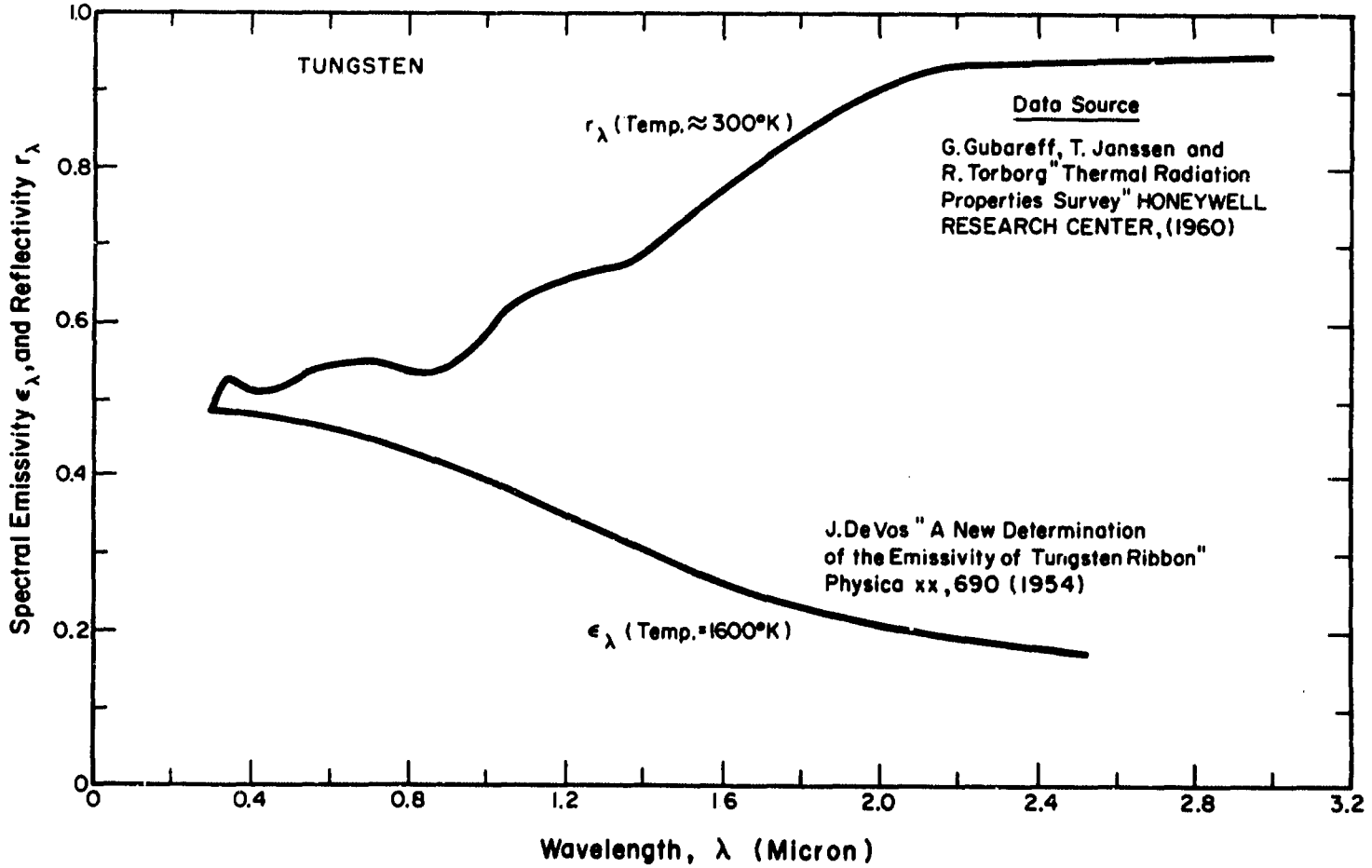

Figure B-5. Spectral Emissivity and Reflectivity of Polished Tungsten.

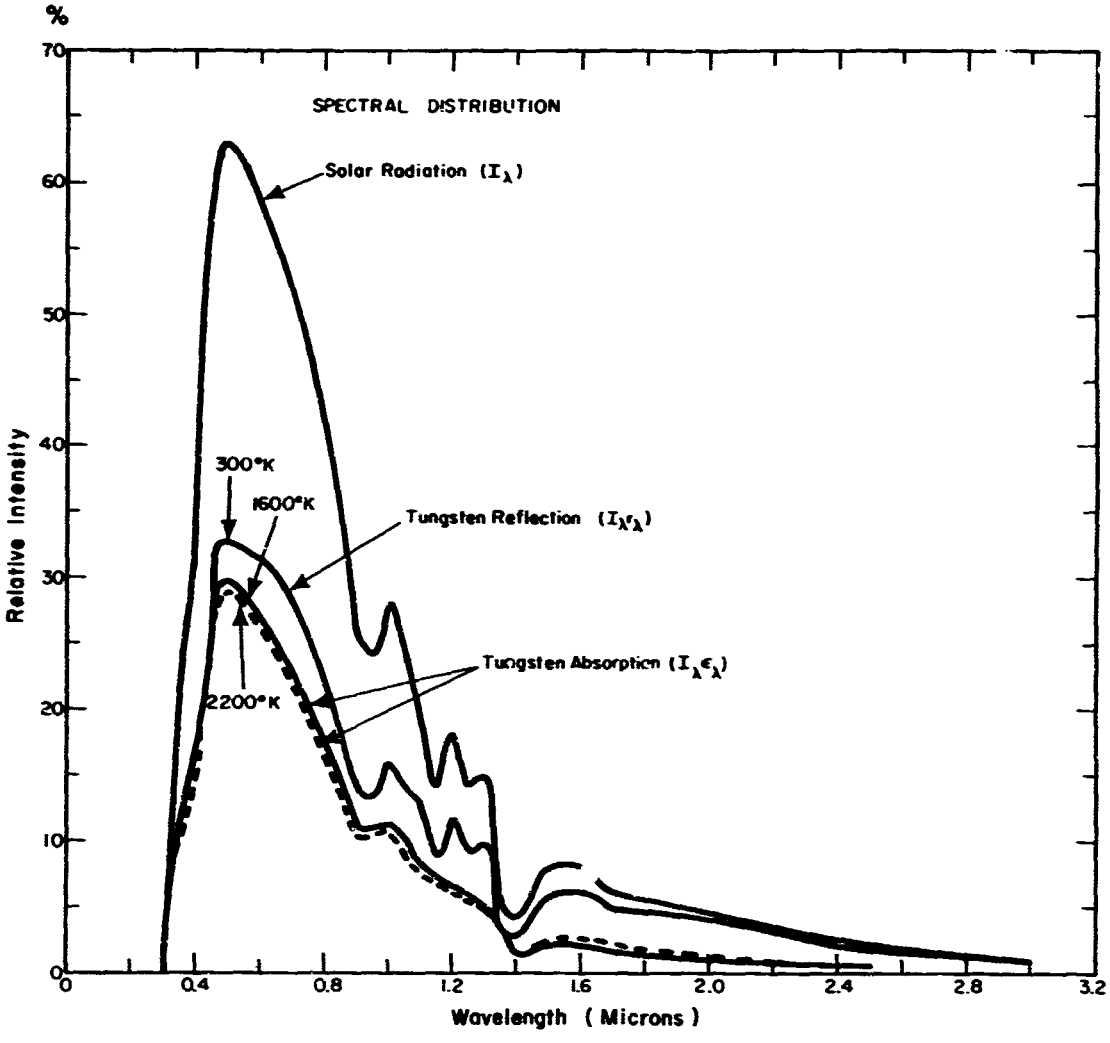

Figure B-6. Relative Intensity of Solar Radiation, Tungsten Reflection and Tungsten Absorption.

APPENDIX C

THERMAL CHARACTERISTICS OF THE CAVITY BACK-PIECE

TEMPERATURE DISTRIBUTION IN THE BACK-PIECE

The design of the back-piece in the generator cavity is discussed in detail in Appendices A and B. The back-piece consists of two parts: the reflector (electropolished W) facing the emitter rear surfaces that form the cavity wall; and the radiator (grooved and Cr_2O_3-coated Mo) that faces a water-cooled copper jacket. The reflector and the radiator are joined together by a high temperature braze (0.65 Pd-0.35 Co) suitable for operation in a high vacuum at temperatures below about 1400°K. The geometry of the reflector, as discussed in Appendixes A and B, is dictated by the optimim solar energy distribution required in the cavity. The geometry of the radiator is governed by the requirement of safe operation of the back-piece and other neighboring parts of the generator under a high vacuum when the conditions of maximum heat transfer are imposed on the back-piece. Under the most unfavorable mirror-cavity arrangement the maximum amount of solar energy that could be absorbed by the back-piece is estimated to be 1800 watts (see analysis in Appendix B). In order to dissipate this power and yet maintain the back-piece at a safe temperature range (e.g., below 1200°K) the rear part, or radiator, must provide a sufficiently large conduction path bounded by an adequate radiation surface. To satisfy these conditions, and also to conform to the size and weight restrictions of the generator, the radiator was designed to assume a partly conical - partly cylindrical shell shape. Dissipation of the absorbed power (1800 watts) by the back-piece takes place only by radiation from three distinct regions (R_1, R_2, and R_3) of the radiator area as shown in Figure C-1. The surfaces of regions R_1 and R_2 are grooved and Cr_2O_3-coated to assume an effective emissivity

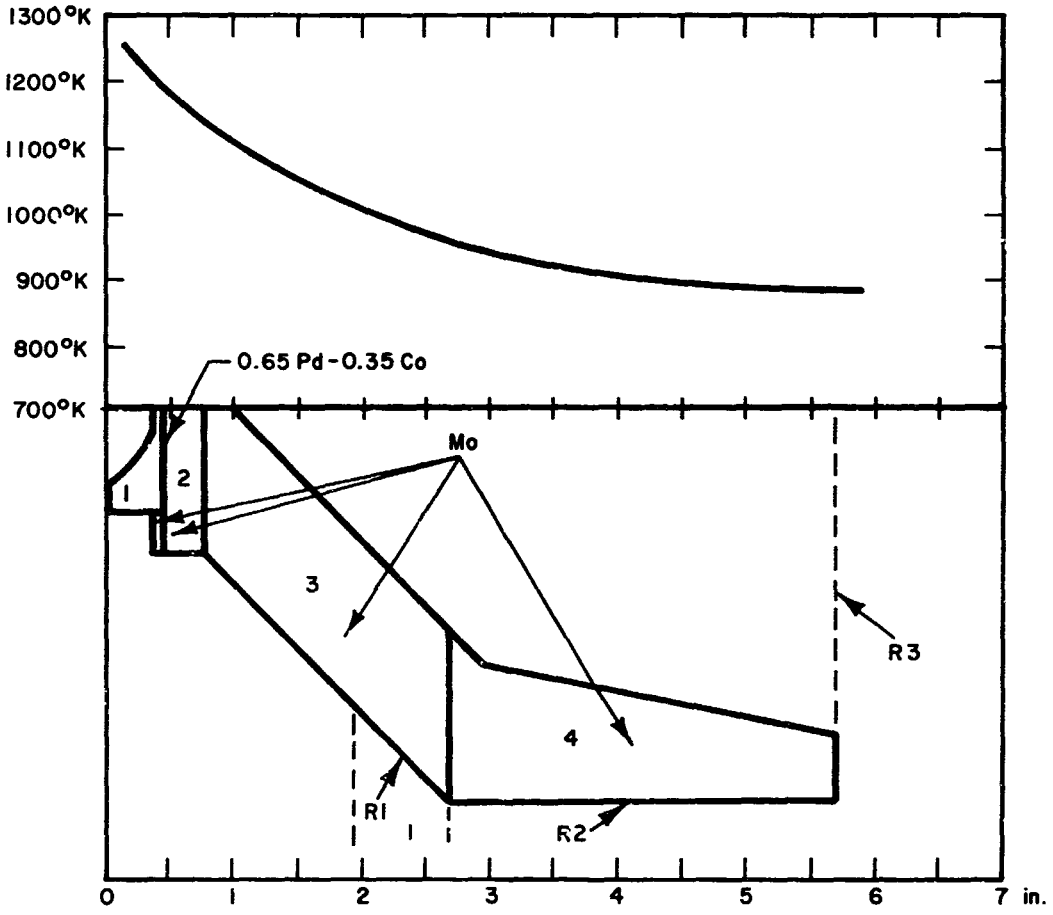

Figure C-1. Temperature Profile in Back-Piece.

of 0.75 (as measured in past experiments). The hollow region R_3 is assumed to radiate only through the area defined by the plane projection of the inside conical surface of the radiator; this area is assumed to have an effective emissivity of nearly 1. Under the above assumptions, the use of an approximation method (rectangular approximation) to solve the heat conduction-radiation equation led to the temperature distribution in the back-piece presented in Figure C-1. It can be readily seen from this figure that when the radiator-reflector interface (brazed section) is at 1200°K the end of the radiator is at 900°K, with the whole radiator surface at an average temperature of 950°K; under these conditions the temperature gradient along the radiator length is about 33°K/inch. The above temperatures were computed for a total radiated power of 1800 watts, with the surroundings (water-cooled, Cr_2O_3 copper jacket) maintained at nearly room temperature (e.g. 300°K). These conditions are satisfied, provided the effective radiator surface (regions R_1, R_2 and R_3) is approximately 76 $in.^2$

REFLECTOR-RADIATOR BRAZE EVALUATION

In the preceding section the assumption was made that the temperature difference across the braze interface was equal to zero. In order to evaluate the validity of this assumption, special tests were performed. These tests involved metallurgical examination of several brazed samples of W and Mo and thermal measurements of one selected braze material. Metallurgical examination of two brazes were performed. These were: (1) 100% Pd, and (2) 65% Pd-35% Co. Metallographs of the brazes were presented to JPL, and the decision was made to perform the thermal tests on the 65% Pd-35% Co braze material.

The basis of this choice was the wettability of the tungsten piece by the braze material.

A direct measurement of the thermal resistance of a very thin braze joint is very difficult because the size of the thermal probe is much larger than the thickness of the braze joint, and the interface temperature cannot be determined accurately. Therefore, a comparison type of measurement was used for this evaluation: i.e., a comparison of the temperature difference between two points in a reference material and the temperature difference observed in a brazed sample under identical conditions of geometry, temperature and heat flux. Such tests were performed for a reference Mo sample and a brazed W-Mo sample. The conclusion of these tests was that the 65% Pd-35% Co braze joint introduces a temperature difference in the actual reflector-radiator interface which does not exceed 1°K per 100 watts. A detailed analysis of the thermal measurements is given below.

TESTS AND RESULTS

The experiment described below was performed in order to determine the temperature gradient across a W-Mo interface with a thin film of 0.65 Pd-0.35 Co brazing alloy providing the thermal conduction path between the W and Mo surfaces. Temperature measurements were taken with iron-constantan thermocouples embedded in the curved surfaces of W and Mo cylinders of identical geometry; the cylinders were brazed together in vacuum with an 0.001-inch-thick disk of an 0.65 Pd-0.35 Co brazing alloy. A photograph of the cylinders and the disk before brazing is shown in Figure C-2; Figure C-3 shows a photograph of the W-Mo specimen after brazing. Each cylinder in the

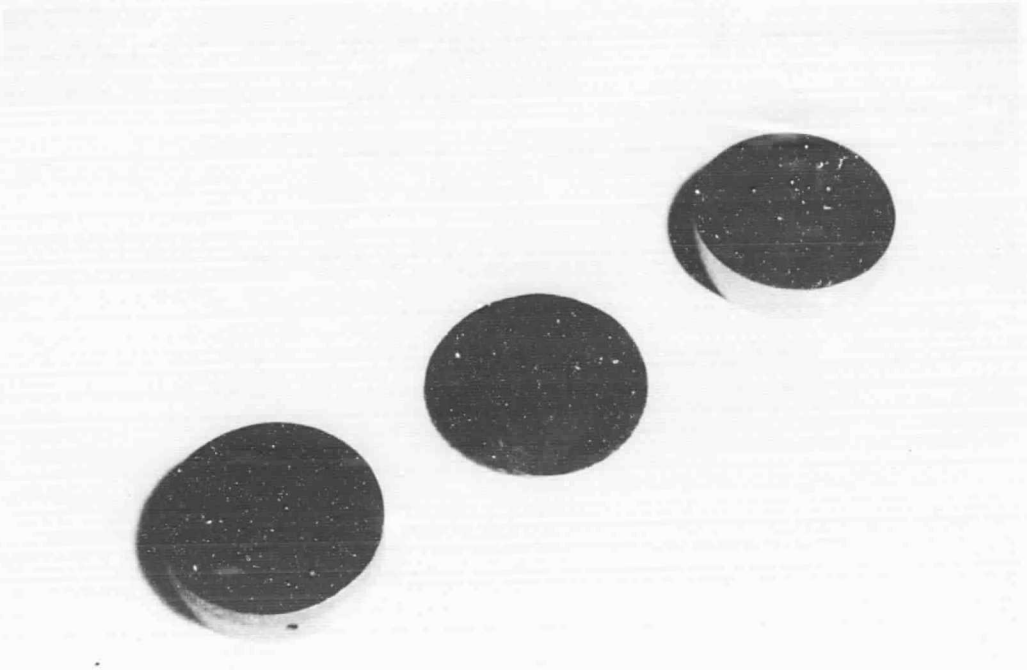

Figure C-2. W, Braze (0.65 Pd-0.35 Co), and Mo Discs Before Forming Test Specimen.

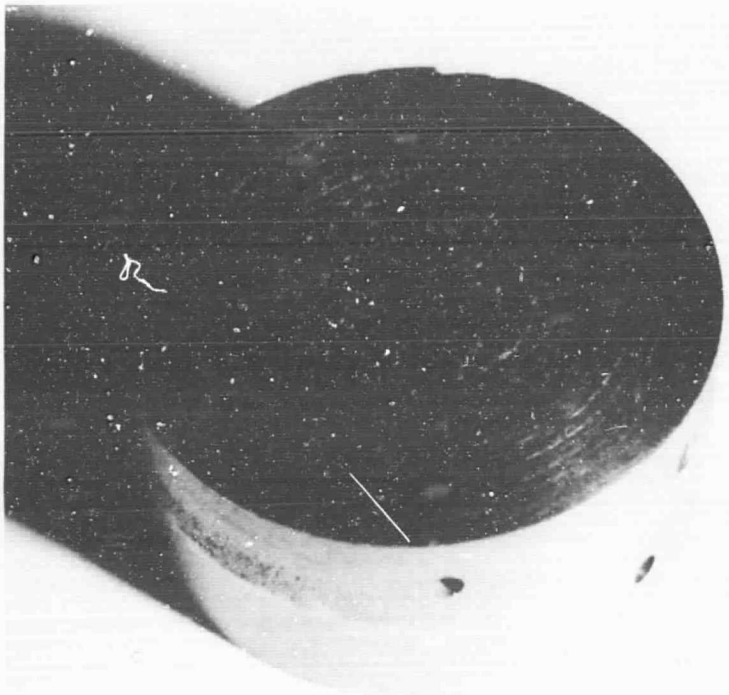

Figure C-3. Completed W-Mo Test Specimen.

specimen has a diameter of 1.106 ± 0.003 inch and a thickness of 0.250 ± 0.002 inch. Three thermocouple holes, each 0.060 ± 0.002 inch in diameter and 0.080 ± 0.003 inch deep, are located on the curved surface of each cylinder, and they are on the same plane, perpendicular to the cylinder axis. The two planes are 0.245 ± 0.002 inch apart, almost equidistant from the W-Mo interface. The three holes in the W cylinder have angular displacement of 90°, 135° and 135°; in the Mo cylinder the holes are placed 135°, 112.5° and 112.5° apart. During assembly the two cylinders were so located that in the completed specimen any two adjacent holes had an angular displacement of either 45° or 67.5°, as shown in the diagram of Figure C-4. The free flat surface of the Mo cylinder in the W-Mo specimen is brazed with an 0.82 Au-0.18 Ni brazing alloy to the flat surface of an OFHC copper cylinder of about 1.250-inch diameter and 0.250-inch thickness. The other flat surface of the copper cylinder is joined with soft solder (0.60 Sn-0.40 Pb) to a copper tube used for circulating water. A thermocouple hole, similar to those in the W-Mo specimen, is located on the curved surface of the copper cylinder. A photograph of the completed specimen is shown in Figure C-5.

Another specimen, similar to the one described above, was assembled and used in the present experiment. In this specimen the W and Mo cylinders were replaced by a one-piece Mo cylinder having practically identical geometry and arrangement of the thermocouple holes. The material in this specimen was obtained from the same raw stock from which the Mo cylinder in the W-Mo specimen was cut. A photograph of the all-Mo specimen is shown in Figure C-6.

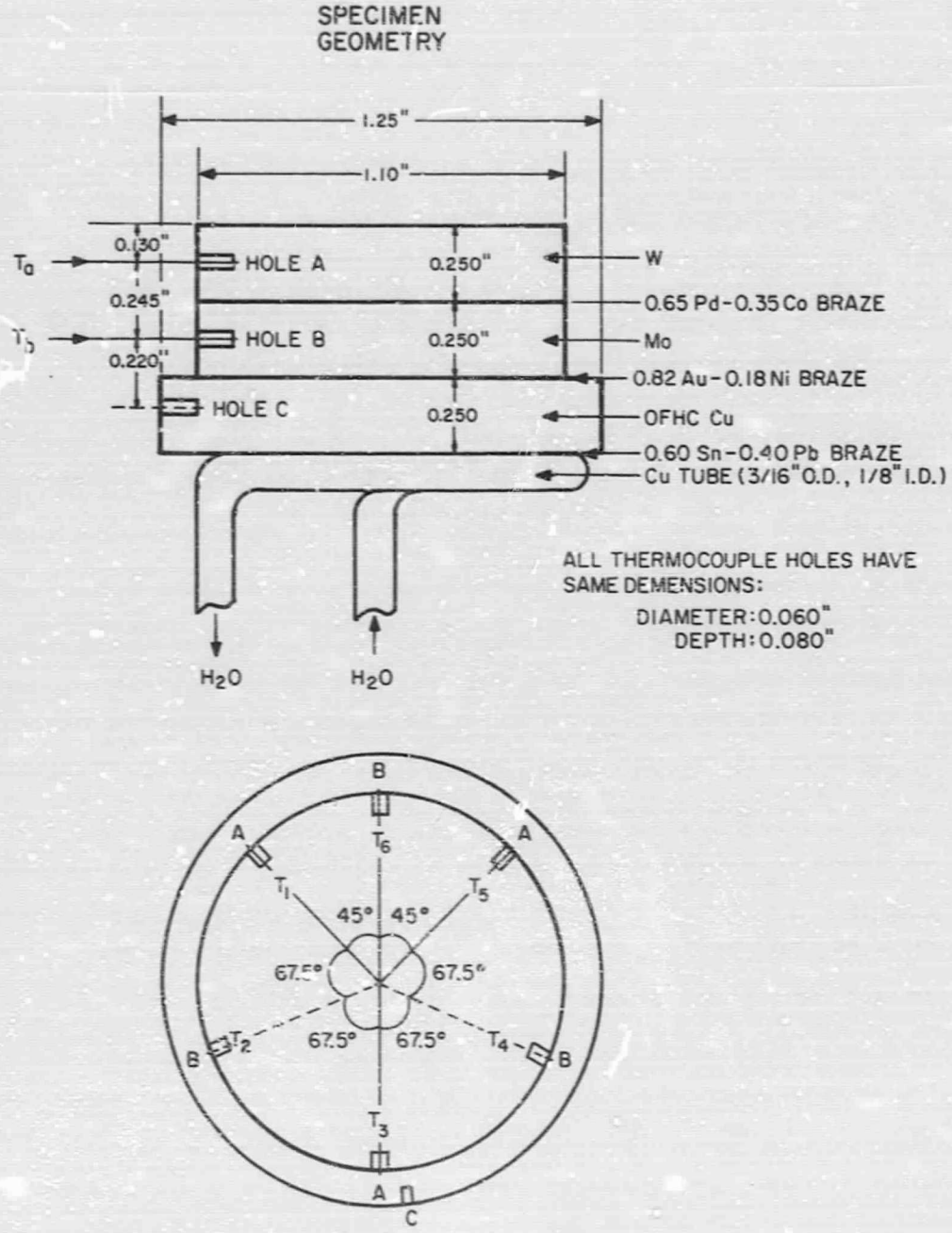

THERMOCOUPLE HOLE ARRANGEMENT AND TEMPERATURE (T) DESIGNATION.

Figure C-4. Schematic of W-Mo Test Specimen.

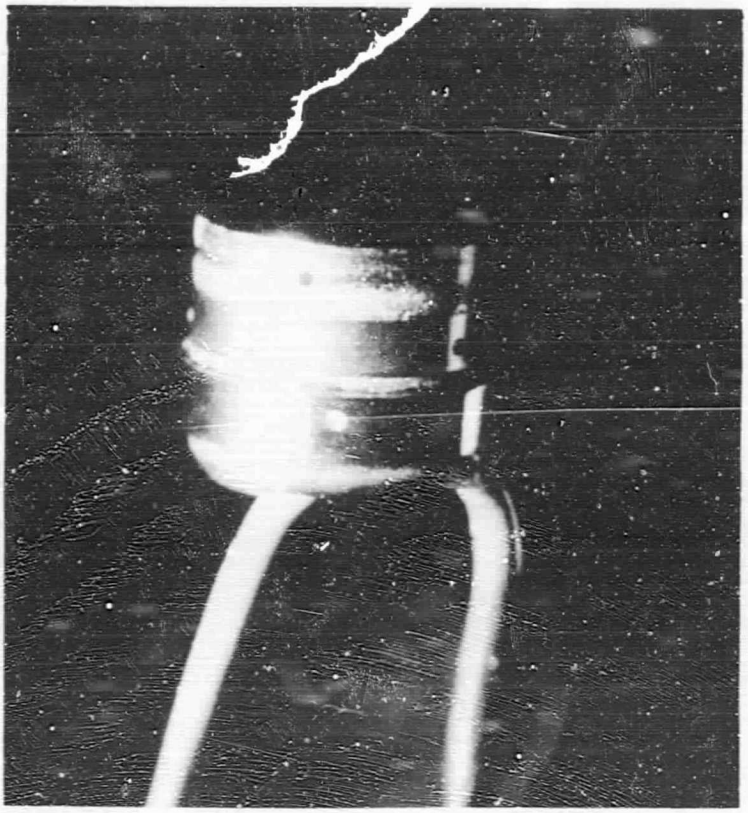

Figure C-5. W-Mo Specimen Brazed on a Water-Cooled Cu Plate.

Figure C-6. All Mo Test Specimen.

The all-Mo specimen was used in this experiment to measure the temperature gradient along a continuous Mo path and compare it with that obtained from the W-Pd/Co-Mo path in the first specimen. Both specimens were tested under identical conditions, using the same heat source and heating arrangement, the same heat sinks, and the same vacuum level. Heat to each specimen was supplied by electron bombardment and radiation from a W filament centrally located directly above the free flat surface of the W cylinder in the first specimen and above that of the Mo cylinder in the second. In both cases the heat was removed by water flowing continuously at a constant rate through a copper pipe brazed to the copper base of each specimen.

The results of the present tests, tabulated in Table C-I, were obtained as follows:

The specimen was mounted on a water-cooled copper tube inside a vacuum bell jar, and an electron-bombardment assembly was placed above the free surface of the specimen (see Figure C-7). Seven iron-constantan thermocouples were connected to the specimen and were checked for differences in room temperature measurements (in both tests no temperature difference greater than 0.5°C was observed between all thermocouples). After the bell jar was evacuated to a pressure of about 2×10^{-5} torr, and with the water flowing through the base of the specimen, the W filament in the electron-bombardment assembly was heated to a given temperature while an electron-accelerating voltage of 1000 volts was applied between the filament assembly and the specimen, which was kept at ground potential (see Figure C-8). When the specimen had reached thermal equilibrium

TABLE C-I

TEMPERATURES OF W-Mo AND ALL-Mo TEST SPECIMENS

	Q_f	Q_e	T_1	T_3	T_5	T_a		T_2	T_4	T_6	T_b	ΔT
	(watt)					(°C)						
	Input Power			W				Mo				W-Mo
W-Mo Specimen	165	158	62	53	68	61		47	45	52	48	13
	175	230	85	75	91	84		62	61	71	65	19
	183	297	102	90	109	100		74	72	83	76	24
	192	332	112	100	122	111		80	77	90	82	29
				Mo					Mo			Mo-Mo
All-Mo Specimen	161	120	50	50	55	52		43	46	42	44	8
	170	195	70	72	78	73		56	60	55	57	16
	178	255	86	89	96	90		68	73	67	69	21
	186	298	97	100	109	102		74	80	74	76	26

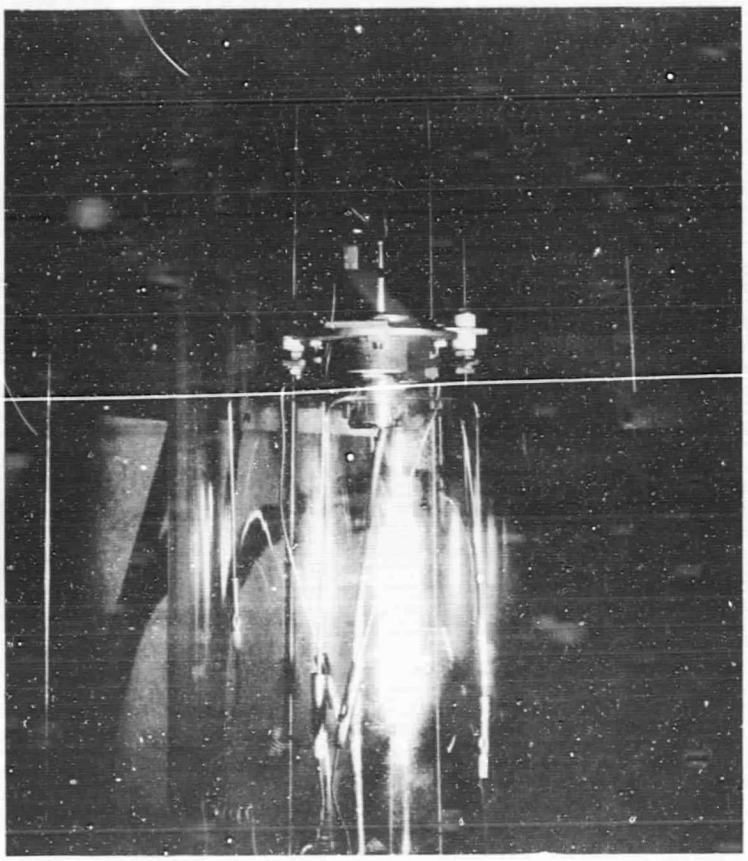

Figure C-7. W-Mo Specimen with Electron-Bombardment Unit Mounted Inside Glass Bell Jar.

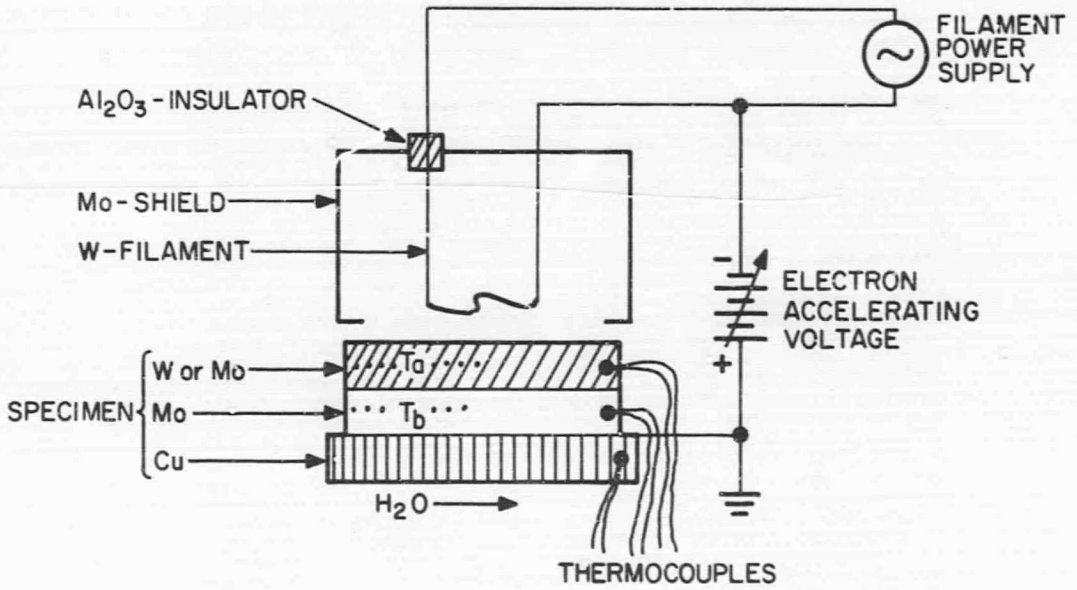

Figure C-8. Test Specimen Heating Arrangement.

the specimen temperatures, and also the electron-bombardment current and the filament input current and voltage, were recorded. From these current and voltage measurements the electron-bombardment input power (Q_e) to the specimen and the filament input power (Q_f) were computed; Q_f and Q_e are tabulated in the first and second columns of Table C-I. The temperatures T_1, T_3 and T_5, measured on the W cylinder in the first specimen and in the upper half (nearer the filament) of the Mo cylinder in the second specimen, were recorded and averaged to give the mean temperature T_a of this section of the specimen. T_1, T_3, T_5 and T_a are shown in the third, fourth, fifth and sixth columns of Table C-I. The temperatures T_2, T_4 and T_6, measured on the Mo cylinder of the W-Mo specimen and the lower part of the all-Mo specimen, were also recorded and averaged to give the mean temperature T_b of that section. T_2, T_4, T_6 and T_b are listed in the seventh, eighth, ninth and tenth columns of Table C-I. The temperature difference $\Delta T = T_a - T_b$ was subsequently computed and tabulated in the eleventh column of Table C-I. These temperature measurements were repeated several times for the same specimen input heat flux (i.e., the same Q_e) to ensure that the specimen was in a state of thermal equilibrium, and thus that the recorded temperatures were representative of that state. During this time Q_f, and subsequently Q_e, varied on certain occasions, due to instrumentation drift, but this variation was too small (i.e., up to 5 watts) to affect the specimen temperatures, which in no case were observed to change by more than 1°C, once the specimen was thermally stabilized.

The experimental procedure described above was repeated for different values of the input power to each specimen, indicated by different values of Q_f and Q_e, as shown in Table C-I. In each case,

temperature measurements were initiated only after each specimen had reached thermal equilibrium.

It should be noted that the differences between the temperatures T_1, T_3 and T_5, and consequently between T_2, T_4 and T_6, observed in the two specimens are primarily due to the asymmetrical form (S-shape) of the filament, which caused a non-uniform distribution of the heat input (electron flux and radiation) to the specimen. This non-uniformity, however, was the same in both specimens, and therefore the average temperatures, T_a and T_b, obtained in the two cases afford direct comparison.

T_b is plotted versus T_a in Figure C-9; it is evident from this plot that in both specimens the temperature difference $(T_a - T_b)$, measured across the same length, is for all practical purposes the same. The electron-bombardment input flux (Q_e) to each specimen and the corresponding filament input power (Q_f) are also plotted versus T_a in Figure C-9. It can be seen from this figure that, for both specimens, Q_e and Q_f are also approximately the same for a given value of T_a. This implies that the filament temperature was the same in both cases for the same value of T_a. Since the position of the filament and the area and condition of the surface of each specimen were almost identical in both tests, the radiation (Q_r) absorbed by each specimen was also the same, assuming that the W and Mo surfaces had the same emissivity. In the temperature range considered here (i.e., 60°C to 140°C) for the specimen surface, the total emissivity (ϵ) of W and Mo varies from about 0.040 to 0.041 and 0.020 to 0.021[1], respectively, and therefore the value of Q_r for W should be slightly larger than for Mo (since $\epsilon_W > \epsilon_{Mo}$). However, this difference in Q_r would not change appreciably the total heat input

---

[1] G. Gubareff, J. Janssen, R. Torberg, "Thermal Radiation Properties Survey," Honeywell Research Center, Minneapolis-Honeywell Regulator Co., Minneapolis, Minnesota (1960).

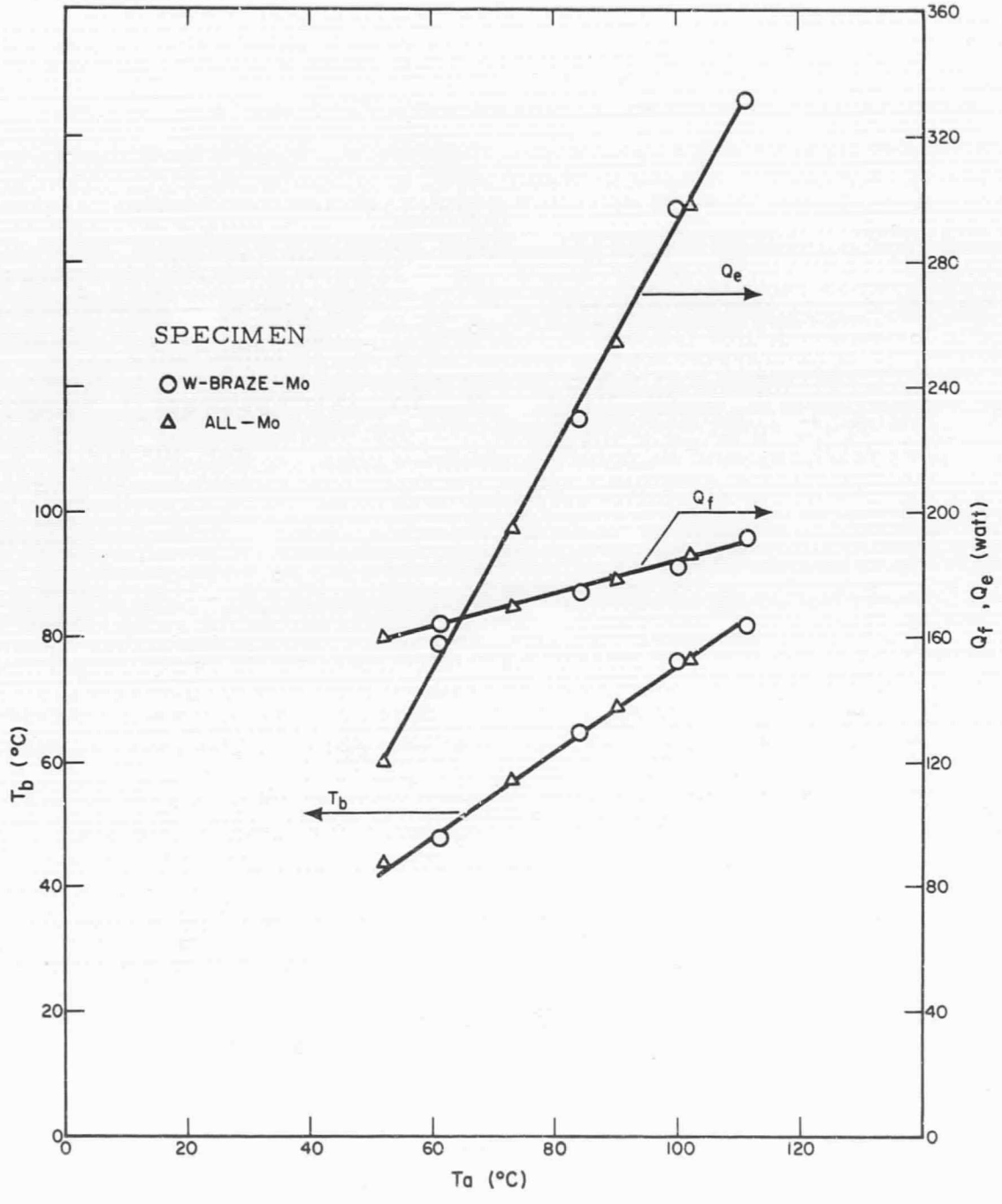

Figure C-9. Plots of Test Specimen Temperature and Input Power.

(Q) to each specimen, since Q_r, as will be shown below, is only a small fraction ($\sim 10\%$) of Q. An estimate of Q can be obtained from the heat flow in the all-Mo specimen, the thermal conductivity (k) of which is accurately known and is constant (1.4 watt/ cm-°C) in the temperature range (50°C - 120°C) of the specimen. Assuming that all the heat (Q) was conducted throughout the entire area (A) of the specimen in the path length (L) across which T_a and T_b was measured, then, in view of the data of Figure C-8, one obtains the following results, listed in Table C-II, from $Q = \frac{kA}{L}(T_a - T_b)$, for $A = 6.15\ cm^2$ and $L = 0.625$ cm; Q_r is computed from $Q_r = Q - Q_e$. Table C-II also presents the filament input power (Q_f), taken from the data of Figure C-9, and the computed ratios Q_r/Q and Q_r/Q_f. In order to check the above results for Q, an estimate of Q_r was obtained from

$$Q_r = F\sigma A_f T_f^4$$

where:

$$F = \left[\frac{1}{G} + \frac{1}{\epsilon_f} - 1 + \frac{A_f}{A}\left(\frac{1}{\epsilon} - 1\right)\right]^{-1}$$

is the radiation exchange factor between the W filament of total emissivity ϵ_f at a temperature T_f and the specimen of total emissivity ϵ at a temperature much smaller than T_f. G is the geometrical view factor between the filament of area A_f and the specimen of area A. The filament temperature is obtained from Dushman's equation:

$$I_e = C_1 A_f T_f^2 \exp\left(-\frac{C_2}{T_f}\right),$$

TABLE C-II

HEAT INPUT IN THE ALL-Mo TEST SPECIMEN

T_a	$T_a - T_b$	Q	Q_e	Q_r	Q_f	$\frac{Q_r}{Q}$	$\frac{Q_r}{Q_f}$
(°C)		(watts)					
60	12	166	151	15	164	0.090	0.091
80	18	248	222	26	174	0.105	0.149
100	24	332	294	38	184	0.114	0.206

where:

$$C_1 = 120 \frac{\text{amp}}{\text{cm}^2 \cdot {}^\circ\text{K}}, \text{ and } C_2 = 52{,}400\ {}^\circ\text{K for W.}$$

The electron current (I_e) was measured directly in these tests and can be deduced from the data for Q_e in Figure C-9, since $I_e = \frac{Q_e}{V_e}$, with the electron-accelerating voltage V_e = 1000 volts, constant in all measurements. From the geometry of the filament (2.8 cm long, 0.076 cm in diam), and its separation (0.635 cm) from the specimen (of 6.15-cm^2 area), the filament area A_f = 0.67 cm^2 and the view factor G = 0.5 were estimated. For the typical value of T_a = 60°C, I_e = 0.150 A (Q_e = 150 watts), and hence $T_f \approx 2130$°C with $\epsilon_f \approx 0.3$.[1] Using ϵ_W = 0.04 and $\epsilon_{Mo} \approx 0.02$ (for a specimen surface temperature near 60°C), one obtains $F_{Mo} \approx 0.104$ and $F_W \approx 0.144$, and subsequently $(Q_r)_{Mo} \approx$ 13 watts and $(Q_r)_W \approx 18$ watts. These results support the data for Q_r (15 watts) and hence for Q obtained for Mo previously and presented in Table C-II, and indicate that $Q_W \gtrapprox Q_{Mo}$. Since $T_a - T_b$ was the same in both specimens, the above results indicate that the thermal resistance of the W-Braze Mo specimen is equal to or smaller than (by a factor of 1.05) the thermal resistance presented by the solid Mo specimen. This difference is attributed to the slightly higher thermal conductivity of W. For comparison, the thermal conductivities[2] of W and Mo are plotted versus temperature in Figure C-10.

---

(2) Purdue University, "Thermophysical Properties Data Book," Volume I (1966).

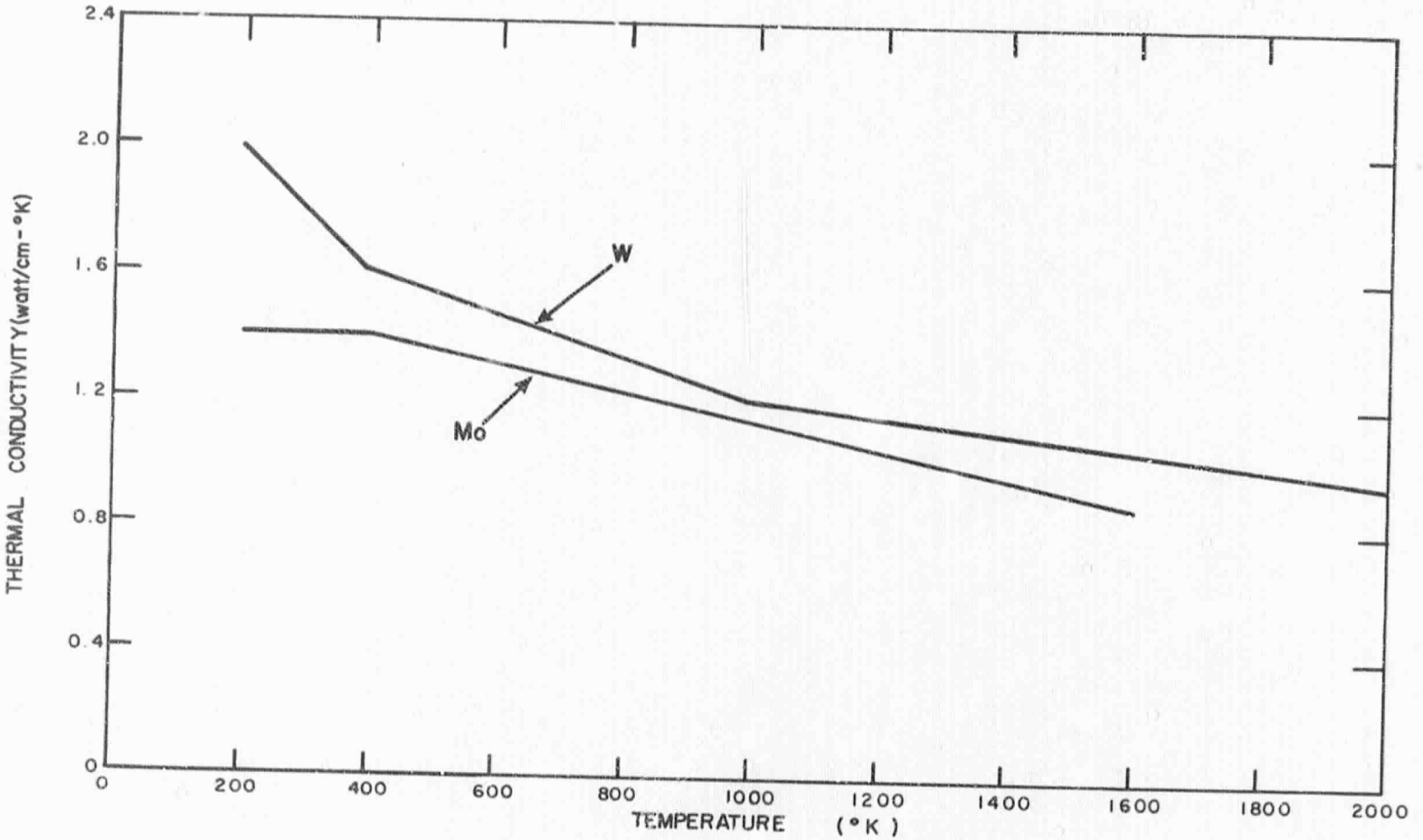

Figure C-10. Plot of Thermal Conductivities of W and Mo.